Complement Factor H Inhibits CD47-Mediated Resolution of Inflammation

Bertrand Calippe, Sébastien Augustin, Fanny Beguier, Hugo Charles-Messance, Lucie Poupel, Jean-Baptiste Conart, Shulong J. Hu, Sophie Lavalette, Alexandre Fauvet, Julie Rayes, et al.

Complement factor H inhibits CD47-mediated resolution of inflammation

Bertrand Calippe[1*], Sebastien Augustin[1*], Fanny Beguier[1], Hugo Charles Messance[1], Lucie Poupel[2], Jean-Baptiste Conart[1], Shulong Hu[1], Sophie Lavalette[1], Alexandre Fauvet[1], Julie Rayes[3], Olivier Levy[1], William Raoul[1], Catherine Fitting[10], Thomas Denèfle[8], Matthew C Pickering[4], Claire Harris[5], Sylvie Jorieux[6], Patrick M. Sullivan[7], José-Alain Sahel [1], Philippe Karoyan[8], Przemyslaw Sapieha[9], Xavier Guillonneau[1], Emmanuel L. Gautier[2], Florian Sennlaub[1†]

[1]Institut de la Vision, 17 rue Moreau, Sorbonne Universités, UPMC Univ Paris 06, INSERM, CNRS, 75012 Paris, France.
[2]Sorbonne Universités, UPMC Univ Paris 06, INSERM UMR_S 1166, Faculté de médecine Pitié-Salpétrière, 91 Boulevard de l'hôpital, 75013, Paris, France.
[3]Université Paris Descartes, Unité Mixte de Recherche en Santé 872, Centre de Recherche des Cordeliers, Paris, France;
[4]Centre for Complement and Inflammation Research, Department of Medicine, Imperial College, London W12 0NN, UK.
[5]Institute of Infection and Immunity, Cardiff University, Cardiff, UK.
[6]LFB Biotechnologies, Lille, France.
[7]Department of Medicine, Centers for Aging and Geriatric Research Education and Clinical Center, Durham Veteran Affairs Medical Center, Duke University, Durham, North Carolina 27710.
[8]Laboratoire des Biomolécules, UMR 7203 and FR 2769, Sorbonne Universités, Université Pierre et Marie Curie, Paris, France; Centre National de la Recherche Scientifique, UMR 7203, Paris, France; Département de Chimie, École Normale Supérieure, Paris, France.
[9]Department of Ophthalmology, Maisonneuve-Rosemont Hospital Research Centre, University of Montreal, Quebec, Canada.
[10]Unité Cytokines & Inflammation, Département Infection et Epidémiologie, Institut Pasteur, 75015 Paris, France.
*these authors have contributed equally

†Correspondence should be addressed to Dr Florian Sennlaub, Inserm, UMR_S 968, Institut de la Vision, Paris, F-75012, France. Tel: (33) 1 53 46 26 93,

Email: florian.sennlaub@inserm.fr.

ABSTRACT

Age-related macular degeneration (AMD) is a highly heritable major cause of blindness characterized by subretinal inflammation. Of all genetic factors, variants of Complement factor H (CFH) are associated with greatest linkage to AMD. Using loss of function genetics and orthologous models of AMD, we provide mechanistic evidence that deficiency in CFH completely prevents pathogenic subretinal accumulation of mononuclear phagocytes (MP) and accelerates resolution of inflammation. We show that MP-persistence arises secondary to binding of CFH to CD11b/CD18, which obstructs physiologically-occurring thrombospsondin-1 (TSP-1)-CD47-mediated elimination of MPs from the subretinal space. The AMD-associated CFH_{402H} isoform markedly increased this inhibitory effect on microglial cells, indicating a causal link to disease etiology. Our findings were confirmed in acute sterile peritonitis. Pharmacological activation of CD47 accelerated resolution of both subretinal and peritoneal inflammation, which may be exploited in the therapy for chronic inflammatory diseases, including AMD.

INTRODUCTION

Age-related Macular Degeneration (AMD) is a highly heritable neuroinflammatory disorder characterized by sizeable deposits of lipoproteinaceous debris called soft drusen (early AMD), choroidal neovascularisation (wet AMD, late form), or by an extending lesion of the retinal pigment epithelium (RPE) and photoreceptors (geographic atrophy, GA, late form) (Ambati et al., 2013; Sarks, 1976). Early AMD affects more than 150 million people worldwide and 10 million patients suffer from late AMD (Wong et al., 2014). AMD is strongly associated with common and rare variants of Complement factor H (CFH), indicating its causal implication in the pathogenesis (Fritsche et al., 2013; Fritsche et al., 2016). The understanding of its mode of action and more generally the origins of AMD remain unclear.

CFH is an abundant soluble plasma factor composed of 20 Short Consensus Repeat domains (SCR) (Kopp et al., 2012) with important roles in inflammation (Kopp et al., 2012; Mihlan et al., 2009), coagulation (Rayes et al., 2014; Vaziri-Sani et al., 2005) and as an antioxidant (Shaw et al., 2012; Weismann et al., 2011). The SCR7 domain of CFH binds to glycosaminoglycans (GAG) on cell surfaces where it inhibits complement activation (Kopp et al., 2012). This domain additionally allows CFH to bind to myeloid cells via the integrin CD11b/CD18 (Complement 3 Receptor, Mac-1) (DiScipio et al., 1998; Losse et al., 2010), supporting myeloid cell adhesion (DiScipio et al., 1998) and migration (Losse et al., 2010) as well as the phagocytosis of microbes (Losse et al., 2010) and cell debris (Kang et al., 2012). At the inflammatory site, CFH is strongly secreted by mononuclear phagocytes (MP), such as microglial cells (MC) and macrophages (Mφ) (Gautier et al., 2012; Luo et al., 2011; Schlaf et al., 2001), adding to the exudated plasma CFH and CFH produced by certain stromal cells such as the retinal pigment epithelium (RPE) in the eye (Anderson et al., 2010).

The substitution of histidine 402 for tyrosine (Y402H) in the SCR7 domain accounts for the major part of the genetic risk of AMD (Fritsche et al., 2014), but is also strongly associated with other conditions such as smoking-associated lung cancer (Zhang et al., 2012) and increased

mortality after cerebral hemorrhage (Appelboom et al., 2011). The association with AMD is found for both advanced forms (Fritsche et al., 2014), but also for early disease stages (Fritsche et al., 2014; Magnusson et al., 2006), suggesting CFH_{402H} drives a pathomechanism implicated at the onset of disease.

Early and advanced forms of AMD are associated with chronic accumulation of MPs in the subretinal space located between the RPE and photoreceptor outer segments (Combadiere et al., 2007; Gupta et al., 2003; Lad et al., 2015; Levy et al., 2015a; Sennlaub et al., 2013). Functional studies in animal models suggest that subretinal MP accumulation play a critical role in neovascularization (Sakurai et al., 2003; Tsutsumi et al., 2003) and photoreceptor degeneration (Combadiere et al., 2007; Cruz-Guilloty et al., 2013; Kohno et al., 2013; Rutar et al., 2012; Sennlaub et al., 2013; Suzuki et al., 2012) that characterize late AMD. Similarly, non-resolving low-grade inflammation and MP persistence, contributes significantly to the pathogenesis of many chronic, age-related diseases, such as metabolic diseases (obesity, atherosclerosis), neurodegenerative diseases (Glass et al., 2010; Sennlaub et al., 2013; Thompson et al., 2007) and cancers (Grivennikov et al., 2010; Hotamisligil, 2010). It is not a primary cause of these diseases, but causes considerable collateral damage to host cells, which fuels further inflammation (Nathan and Ding, 2010). In this study, we describe for the first time a noncanonical role of complement factor H (CFH) in the control of the MP population in the resolution of acute- and chronic-inflammation. Our study reveals a general mechanism of inflammation resolution and shows how the major AMD-predisposing CFH variant fuels non-resolving pathogenic sub-retinal inflammation (Nathan and Ding, 2010; Combadiere et al., 2007; Gupta et al., 2003; Lad et al., 2015; Levy et al., 2015a; Sennlaub et al., 2013).

RESULTS

CFH deficiency prevents chronic pathogenic subretinal inflammation

Physiologically, the subretinal space is devoid of immune cells, including resident MCs (Combadiere et al., 2007; Gupta et al., 2003 ; Lad et al., 2015; Levy et al., 2015a; Penfold et al., 2001), due to the potent immunosuppressive pro-apoptotic factors produced by the RPE that eliminate infiltrating leukocytes (Griffith et al., 1995; Levy et al., 2015a). We have previously shown that high levels of Apolipoprotein E, as observed in subretinal MPs of AMD patients (Levy et al., 2015a), *Cx3cr1*-deficient mice (Levy et al., 2015a) and humanized transgenic mice expressing the AMD-risk APOE2 isoform (TRE2-mice), induce chronic, age-related and pathogenic subretinal MP accumulation (Levy et al., 2015a; Levy et al., 2015b; Sennlaub et al., 2013). Indeed, *Cx3cr1*$^{GFP/GFP}$ and *TRE2* mice model the age-dependent subretinal MP accumulation and associated photoreceptor degeneration observed in human AMD (Combadiere et al., 2007; Levy et al., 2015b; Sennlaub et al., 2013). We therefore sought to determine whether *Cfh* deficiency would alter disease onset and progression in *Cx3cr1*$^{GFP/GFP}$ and *TRE2* mice. Quantification of subretinal IBA-1^{+} MPs on retinal and RPE/choroidal flatmounts of 2-3 month and 12 month old animals showed that the age-related increase in subretinal MPs observed in both models was nearly completely blunted in the absence of CFH (Fig. 1A and 1B). Micrographs revealed that *Cx3cr1*$^{GFP/GFP}$ *Cfh*$^{-/-}$ mice were protected against the thinning of the outer nuclear layer, which hosts photoreceptor nuclei, usually observed in *Cx3cr1*$^{GFP/GFP}$ mice (Sennlaub et al., 2013) (Fig. 1C). Photoreceptor nuclei row counts (Fig. 1D) and calculation of the area under the curve showed *Cfh* deficiency protected against the photoreceptor cell loss observed in *Cx3cr1*$^{GFP/GFP}$ mice (Fig. 1E) and *TRE2*-mice (Levy et al., 2015b) (Fig. 1F), while no difference was observed in *Cfh*$^{-/-}$ compared to control-mice. Similarly, *Cfh* deficiency completely protected against cone loss observed on peanut agglutinin / cone arrestin stained retinal flatmounts from 12m-old *Cx3cr1*$^{GFP/GFP}$ mice and TRE2-mice (Fig. 1G-J). It had no effect on key pathogenic cytokine secretion of MPs *in vitro* (Fig. S1),

suggesting that the numerical increase rather than differences in polarization provokes the degeneration. Thus, we show CFH is required for the chronic, age-related subretinal MP accumulation and associated photoreceptor degeneration observed in both mouse models of AMD. A similar age- and CFH-dependent increase in MPs was also described in the choroid of *Cfh*$^{+/-}$ compared to *Cfh*$^{-/-}$ mice (Toomey et al., 2015). In humans, ocular CFH immunoreactivity is invariably stronger in AMD donor tissues (Hageman et al., 2005; Johnson et al., 2006; Shaw et al., 2012; Weismann et al., 2011) and CFH autoantibodies are protective in AMD (Dhillon et al., 2010). Together with these observations, our results strongly suggest CFH critically controls subretinal MP accumulation in AMD.

CFH inhibits the resolution of acute subretinal inflammation

Next, to better understand how CFH controls subretinal inflammation, we evaluated its impact on acute light-induced stress. The intensity of the light-challenge model used herein was calibrated to induce substantial subretinal MP infiltration in AMD-prone *Cx3cr1*$^{GFP/GFP}$ and *TRE2* mice but not in *C57BL6/J* controls (Levy et al., 2015b; Sennlaub et al., 2013). Quantification of subretinal IBA-1^{+} MPs revealed similar early subretinal MP accumulation in *TRE2 Cfh*$^{-/-}$ (Fig. 2A) and *Cx3cr1*$^{GFP/GFP}$ *Cfh*$^{-/-}$ mice (Fig. 2B) and their respective controls at the end of the four-day light-challenge. However, after an additional 10 days under normal light conditions to allow for MP clearance and inflammation resolution (Hu et al., 2015), subretinal MPs were eliminated significantly faster in *TRE2 Cfh*$^{-/-}$ and *Cx3cr1*$^{GFP/GFP}$ *Cfh*$^{-/-}$ mice compared to controls (Fig. 2A and B). Thus, our data suggest that CFH controls MP persistence at the inflammatory site rather than their initial accumulation.

Similar to *Cfh*$^{-/-}$ mice (Pickering et al., 2002), *Cx3cr1*$^{GFP/GFP}$ *Cfh*$^{-/-}$ and *TRE2 Cfh*$^{-/-}$ mice have low circulating levels of complement factor C3 (Fig. S2), likely due to un-inhibited plasma complement activation and exhaustion. To test whether the systemic lack of C3 would accelerate the elimination of subretinal MPs as observed in *Cx3cr1*$^{GFP/GFP}$ *Cfh*$^{-/-}$ mice, we

replaced hepatic CFH using hydrodynamic injection of a plasmid encoding *Cfh* under the albumin promoter. Liver CFH complementation restored circulating C3 concentrations in *Cx3cr1*$^{GFP/GFP}$ *Cfh*$^{-/-}$ mice to 40-60% of the *Cx3cr1*$^{GFP/GFP}$ levels over the 14 days of the experimental protocol (Fig. 2C). However, the significant increase in circulating C3 did not affect the number of subretinal MPs in *Cx3cr1*$^{GFP/GFP}$ *Cfh*$^{-/-}$ mice at day 14 (Fig. 2D).

The comparable subretinal MP counts at the beginning of acute inflammation (day 4) (Fig. 2A and B) and the lack of influence of circulating C3 levels during the resolution phase (Fig. 2D) suggested that systemic C3 was not involved in MP recruitment or their elimination. We next assessed relative *Cfh* mRNA levels in retinal and RPE/choroid tissue homogenates, bone marrow (BM-Mos) and circulating (Mos) monocytes as well as MCs isolated from the brain and retina. Our data showed that RPE/choroid and MCs expressed the highest levels of *Cfh* mRNA in WT and *Cx3cr1*$^{GFP/GFP}$ mice (Fig. 2E), in accordance with CFH protein localization around subretinal MPs *in vivo* (Fig. S2). To evaluate whether MCs- or RPE-derived CFH would impact subretinal MP elimination, we adoptively transferred CFSE-labeled MCs from different mouse strains into the subretinal space of either WT or *Cfh*$^{-/-}$ mice. The surviving CFSE^{+} MCs were then enumerated 24h after injection. We previously showed that subretinally injected WT Mos, MCs or Mϕs quickly undergo apoptosis and are eliminated (Levy et al., 2015a), and that such clearance was significantly delayed when MPs lacked CX3CR1 (Levy et al., 2015a). We found *Cx3cr1*$^{GFP/GFP}$ MCs lacking *Cfh* were eliminated faster than controls (Fig. 2F). This difference could be reversed by human CFH (Fig. 2F). Experiments using BM-Mos revealed comparable results (Fig. S3). Interestingly, recipient derived-CFH only had a very minor impact on MCs elimination (Fig. 2F), suggesting MP-derived CFH is more important. Similarly, *TRE2 Cfh*$^{-/-}$ MCs injected in WT recipients were eliminated faster than controls, and adding CFH protein again reversed the effect (Fig. 2G).

In summary, our data show that CFH does not influence initial MP recruitment but inhibits MP elimination during inflammation resolution. They also demonstrate that RPE- and liver-derived CFH have little influence on this phenotype. Indeed, MP-derived CFH is sufficient to inhibit MP clearance. Similar to our experiments, the observation that recipient, but not liver *Cfh* genotype, confers the AMD-risk in liver transplant patients (Khandhadia et al., 2013) suggests that plasma CFH is not involved in AMD pathogenesis and points to the importance of MP-derived CFH in the disease.

CFH binding to CD11b/CD18 inhibits TSP-1/CD47 mediated MP elimination

CFH can act as a cofactor of complement factor I (CFI) to cleave C3b into iC3b, thereby inactivating the C3 convertase that is formed by C3b and activated complement factor B (CFB), while opsonizing apoptotic bodies with increased iC3b (Martin and Blom, 2016). However, the absence of C3 or activated C3 fragments in subretinal MPs of *Cx3cr1*$^{GFP/GFP}$ or *Cx3cr1*$^{GFP/GFP}$ *Cfh*$^{-/-}$ mice (Fig. S2) and low levels of *C3* mRNA in MCs and undetectable transcription of *Cfi* mRNA in MCs and BM-Mos (Fig. S4) and make a significant implication of locally produced C3, C3b, or iC3b in CFH-mediated inhibition of MP elimination unlikely.

CFH also binds directly to the integrin CD11b/CD18 (DiScipio et al., 1998; Kang et al., 2012; Losse et al., 2010) that is strongly expressed in MPs with no detectable differences in our different mouse strains (Fig. S5). Flow cytometry analysis showed fluorescently labeled CFH binds dose-dependently to MCs (Fig. 3A) and BM-Mos isolated from *Cx3cr1*$^{GFP/GFP}$ *Cfh*$^{-/-}$ mice (Fig. 3B). Pre-incubation with an anti-CD11b antibody inhibited CFH binding (Fig. 3B), as previously demonstrated for neutrophils (DiScipio et al., 1998). As shown above (Fig. 2F), adding CFH to *Cx3cr1*$^{GFP/GFP}$ *Cfh*$^{-/-}$ MCs transferred subretinally in WT recipients delayed their elimination. This effect was no longer observed when transferred MPs were treated with the anti-CD11b antibody (Fig. 3C). The antibody also significantly accelerated the elimination of CFH-competent *Cx3cr1*$^{GFP/GFP}$ MCs, contrary to an anti-C3b/iC3b/C3c antibody that inhibits

complement-induced hemolysis (clone 3/26 (Mastellos et al., 2004), Fig. 3C). These results show that CFH binding to the CD11b/CD18 integrin complex is necessary to inhibit MC elimination and suggest a C3-independent, non-canonical role of CFH in the mechanism.

CD11b/CD18 co-localizes with the integrin-associated protein (IAP, CD47) in lipid-rafts (Pfeiffer et al., 2001), a thrombospsondin 1 (THBS1, TSP-1) receptor known to potentiate FasL-induced endothelial cell and T cell death (Manna et al., 2005; Quesada et al., 2005). We therefore investigated whether CFH binding to CD11b/CD18 could limit CD47 activation and impair MP elimination in *Cx3cr1*$^{GFP/GFP}$ and *TRE2* mice (the expression level of TSP-1 and CD47 and the plasma TSP-1 levels were similar in our different mouse strains, Fig. S5). First, proximity ligation assay revealed numerous CD11b/CD47 complexes on *Cx3cr1*$^{GFP/GFP}$ *Cfh*$^{-/-}$ MCs (Fig. 3D). We next analyzed the role of CD47 in subretinal MC clearance in adoptive transfer experiments. Subretinally injected CFSE-labeled MCs from WT, *Thbs1*$^{-/-}$ or *Cd47*$^{-/-}$ donors into WT recipients revealed MCs lacking *Thbs1* or *Cd47* have slower elimination rates than WT MCs (Fig. 3E). Co-injected recombinant TSP-1 accelerated the elimination of WT MCs, reversed the phenotype of *Thbs1*-deficient MCs but had no effect on MCs lacking *Cd47* (Fig. 3E), suggesting the interaction of TSP1 with CD47 mediates MC elimination. Moreover, analysis of *Thbs1*$^{-/-}$ and *Cd47*$^{-/-}$ mice revealed a significant age-related (Fig. 3F) and light-induced (Fig. 3G) increase in subretinal MPs in these strains as compared to controls, but not in mice lacking *Cd36*, an alternative TSP-1 receptor. Overall, our results point to TSP-1/CD47 signaling as central in the maintenance of subretinal immunosuppression, and likely explains the previously reported increased and prolonged subretinal inflammation observed in *Thbs1*$^{-/-}$ mice (Chen et al., 2012; Ng et al., 2009; Wang et al., 2012). Interestingly, binding of TSP-1 to CD36 that mediates endothelial cell apoptosis (Jimenez et al., 2000) and is necessary for latent TGF-β activation (Yehualaeshet et al., 1999) had no significant influence on subretinal MP accumulation, as observed here in *Cd36*$^{-/-}$ mice.

Taking into account the opposing effects of TSP1 and CFH, we next evaluated their interaction in MP elimination. Using our adoptive transfer assay, we found a TSP-1 blocking antibody reversed the accelerated elimination of *Cx3cr1*$^{GFP/GFP}$ *Cfh*$^{-/-}$ MCs compared to controls (Fig. 3H). Furthermore, the faster elimination rate observed after supplementation of recombinant TSP-1 to *Cx3cr1*$^{GFP/GFP}$ *Cfh*$^{-/-}$ MCs was completely lost when purified CFH was concomitantly added (Fig. 3I).

Next, we used the laser-injury model to test whether CFH binding to CD11b or CD47 activation can accelerate inflammation resolution in CFH-competent *Cx3cr1*$^{GFP/GFP}$ mice. Using this model, we take advantage of the fact that laser burn induces a thinning of the retina above the impact, facilitating diffusion of intravitreally-injected molecules to the subretinal space. Our results showed the intravitreal injection at the height of laser-induced subretinal inflammation (d4 and d7) of recombinant TSP-1 (Fig. 3J), CD47-activating peptide PKHB1 (a derivate of the 4N1K CD47-agonist peptide with improved pharmacological properties (Martinez-Torres et al., 2015), Fig. 3K), or the anti-CD11b antibody (that blocks CFH binding to CD11b, Fig. 3L) all significantly accelerated subretinal MP elimination as compared to their controls.

Taken together, our data show that CFH binding to the integrin CD11b/CD18 inhibits subretinal MC elimination. We demonstrate that CD47 co-localizes with CD11b/CD18 on MPs and mediates the physiological role of TSP-1 in subretinal MP elimination. The observation that TSP-1 blockade reversed the effect of CFH deficiency and that recombinant CFH blocks the effect of TSP-1 on subretinal MP elimination strongly suggests that CFH binding to CD11b/CD18 interferes with TSP-1/CD47 signaling. We show that TSP-1 and more specifically CD47 activation efficiently accelerates MP elimination similar to *Cfh*-deficiency.

CFH inhibits the resolution of acute sterile peritonitis

Non-resolving inflammation contributes significantly to the pathogenesis of many chronic, age-related diseases (Nathan and Ding, 2010). To test whether CFH influences inflammation resolution in other pathological contexts, we used a model of acute thioglycollate-induced peritonitis, characterized by an early accumulation of neutrophils, followed by recruited monocyte-derived inflammatory macrophages (recMφ), both experiencing an apoptosis-driven elimination at different kinetics (Gautier et al., 2013). Analysis of the ImmGen dataset (Gautier et al., 2012) (GenBank no. GSE37448) shows *Cfh* mRNA levels in thioglycollate-elicited peritoneal recMφ is approximately doubled compared to circulating blood Ly-6C^{+} Mo, from which they derive (Fig. 4A). Thus, recMφs likely participate to local CFH in peritonitis, in addition to extravasated plasma CFH. Quantification of recruited CD115^{+} F4/80^{+} ICAM2^{lo} recMφs in *Cfh*$^{-/-}$ mice and controls (Fig. 4B), revealed a robust and similar early accumulation 1 day after peritonitis induction (Fig. 4C). At day 3 however, while the numbers of recMφs continued to rise in WT mice, they had receded by 50% in *Cfh*$^{-/-}$ mice (Fig. 4C). This observation was similar to the accelerated elimination of subretinal MPs observed in light-challenged *TRE2 Cfh*$^{-/-}$ and *Cx3cr1*$^{GFP/GFP}$ *Cfh*$^{-/-}$ mice (Fig. 2A and B). Human recombinant CFH injected into the peritoneal cavity of *Cfh*$^{-/-}$ mice at day 1 significantly inhibited the enhanced clearance of recMφs observed in this strain at day 2 as compared to heat-denatured CFH (Fig. 4D), akin to the effect we observed in subretinally injected *Cx3cr1*$^{GFP/GFP}$ *Cfh*$^{-/-}$ MCs (Fig. 2F). In addition, similar to our results in MCs (Fig. 3D), a proximity ligation assay revealed numerous and specific CD11b/CD47 complexes in WT recMφ retrieved at day 1 (Fig. 4E). Finally, a single intra-peritoneal injection of recombinant TSP-1 or the CD47-specific activating peptide PKHB1 at day 1 significantly accelerated the elimination of recMφs as observed at day 2 (Fig. 4F).

In summary, our results show that CFH inhibits recMφ elimination in sterile peritonitis confirming findings for infiltrating MPs in the subretinal space. The observation that

CD11b/CD47 complexes are present on peritoneal recMφ and that CD47 activation accelerates recMφ elimination during peritonitis strongly suggests that CFH inhibits CD47-dependent inflammation resolution similarly in both the eye and the peritoneum.

The CFH_{402H} variant inhibits subretinal MC elimination more potently than the common CFH_{Y402}

The substitution of histidine 402 for tyrosine (Y402H) in CFH sequence accounts for a major part of the genetic risk of AMD. To test whether the Y402H polymorphism influenced the elimination of distinct MPs differently, we transferred CFSE-labeled *Cx3cr1*$^{GFP/GFP}$ *Cfh*$^{-/-}$ MCs or BM-Mos to the subretinal space together with purified CFH_{Y402} or the disease associated CFH_{402H} to WT mice. $CFSE^{+}$ cell counts after 24h revealed that both isoforms inhibited clearance of BM-Mos (Fig. 5A) and MCs (Fig. 5B) compared to cells injected without CFH. However, while CFH_{Y402} and CFH_{402H} had similar effects on BM-Mo elimination (Fig. 5A), CFH_{402H} limited MC clearance by 37% compared to CFH_{Y402} (Fig. 5B). In addition, recombinant CFH_{Y402} reversed the accelerated elimination rate observed when subretinally injected *Cx3cr1*$^{GFP/GFP}$ *Cfh*$^{-/-}$ MCs were treated with recombinant TSP-1, and recombinant CFH_{402H} was 50% more potent at inhibiting this phenomenon (Fig. 5C).

Taken together our results show that CFH_{402H} was significantly more potent to inhibit the subretinal elimination of certain MPs, such as MCs. The CFH_{402H} variant might thereby spur non-resolving inflammation under the retina, and thus explain its association with early and late AMD (Fritsche et al., 2014; Magnusson et al., 2006) where subretinal MPs accumulate(Combadiere et al., 2007; Gupta et al., 2003; Lad et al., 2015; Levy et al., 2015a; Sennlaub et al., 2013).

DISCUSSION

We report the previously unknown ability of CFH to favor subretinal MP accumulation in mice developing chronic, non-resolving, age-related inflammation in the eye. We extended this finding to inflammation resolution in general by using models of acute inflammation in the

peritoneum and the eye. Our work supports the long-standing association between CFH variant and AMD, and we uncovered the mechanisms by which CFH impacts MP infiltration, independently from its action in the complement cascade.

The subretinal space is prone to MP infiltration due to light-induced oxidative stress and high metabolic activity (Combadiere et al., 2007; Ng and Streilein, 2001; Suzuki et al., 2012), and this is physiologically counterbalanced by the expression of immune-suppressive factors by the RPE (Griffith et al., 1995; Levy et al., 2015a). We show that CFH favors MP accumulation by inhibiting their TSP-1/CD47-mediated elimination. Remarkably, *Thbs1*$^{-/-}$ and *Cd47*$^{-/-}$ mice develop age-related subretinal inflammation under normal living conditions. This can possibly be explained by the sensitizing role of TSP-1 on FasL-induced cell death (Manna et al., 2005; Quesada et al., 2005) as FasL expression by the RPE is necessary to prevent subretinal MP accumulation (Griffith et al., 1995; Levy et al., 2015a).

CFH is expressed at high levels in MCs and Mo-derived Mφs in peritonitis and we confirmed a step-wise binding interaction between CFH and CD11b/CD18 (Gautier et al., 2012; Luo et al., 2011; Schlaf et al., 2001) and CD11b and CD47 (Pfeiffer et al., 2001) on MPs. CFH ligation to CD11b/CD18 might thereby sterically hinder the ligation of TSP-1 to CD47 , and increase MP lifespan. Complement activation or CFH-dependent production of iC3b, an alternative ligand of CD11b/CD18, did not play a detectable role in the process, as C3b/iC3b/C3c fragments were not found in the subretinal space and CFI (necessary to produce iC3b) is not significantly transcribed in MPs. A specific antibody that inhibits C3-dependent hemolysis (Mastellos et al., 2004) did not accelerate MP elimination.

In addition, we found that the AMD-associated CFH_{402H} variant has an increased capacity to inhibit the elimination of certain MP populations, such as MCs, strengthening the causal link to AMD etiology. Although CFH_{402H} affinity is decreased to certain GAG species, it is higher in particular to GAG sulfates (Clark et al., 2006). GAG sulfate profiles differ greatly between

MPs and different microenvironments. For example, keratan sulfate proteoglycans (KPSG) are strongly present on ramified brain MCs but not on blood Mos (Wilms et al., 1999). The differential expression of GAG sulfates, such as KPSG, on MCs (Wilms et al., 1999) might explain why CFH_{402H} differentially influences MC but not BM-Mos elimination. Subretinal MPs originating from infiltrating Mo and MCs (Sennlaub et al., 2013) invariably express KPSG strongly (Combadiere et al., 2007; Ng and Streilein, 2001; Ng et al., 2009). This is also the case in spinal cord injury [53], but not in autoimmune neuritis (Jones and Tuszynski, 2002; Matsui et al., 2013). CFH_{402H} might therefore have a particularly strong influence on subretinal inflammation observed in AMD but not necessarily in other chronic inflammatory diseases. In human evolution, the limited elimination of MPs and the increased inflammatory reaction associated with CFH_{402H} might have increased survival to certain infectious diseases, leading to its high frequency as observed today in certain populations. In AMD, CFH_{402H} might be pathogenic as it fuels subretinal inflammation and leads to chronic inflammation, which add to its decreased capacity to inhibit oxidative stress (Shaw et al., 2012; Weismann et al., 2011) and to bind to Bruchs membrane (Clark et al., 2010) that protects the RPE against uncontrolled complement activation (Coffey et al., 2007; Toomey et al., 2015).

Current anti-inflammatory therapies, such as steroids, non-steroidal anti-inflammatroy drugs (NSAID), or immunosuppressive drugs (Ciclosporin) can have paradoxical effects on macrophage function. They increase proinflammatory mediators (high-dose steroids) (Lim et al., 2007), upregulate toll-like receptors on macrophages (Ciclosporin) (Tedesco and Haragsim, 2012) and prolong macrophage infiltration (NSAID) (Gilroy et al., 1999), which might explain their lack of therapeutic effect in AMD. Our findings introduce a new strategy to directly induce the elimination of resilient macrophage accumulation in AMD, and possibly other conditions, by pharmacological activation of CD47.

Acknowledgments:

This work was supported by grants from INSERM, ANR Geno 2009 (R09099DS), ANR MACLEAR (ANR-15-CE14-0015-01), LABEX LIFESENSES [ANR-10-LABX-65] supported by the ANR (Investissements d'Avenir programme [ANR-11-IDEX-0004-02]), Carnot, and ERC starting Grant (ERC-2007 St.G. 210345), the Association de Prévoyance Santé de ALLIANZ, and a generous donation by Doris and Michael Bunte.

Materials and Methods:

Animals

Cfh$^{-/-}$ and targeted replacement mice that express human APOE isoforms (TRE2, TRE3) were generous gifts from Mathew Pickering and Patrick Sullivan, respectively. *Cx3cr1*$^{GFP/GFP}$, *Thbs1*$^{-/-}$, *Cd47*$^{-/-}$, and *Cd36*$^{-/-}$ mice were purchased (Charles River Laboratories, Jackson laboratories) and *Cx3cr1*$^{GFP/GFP}$ *Cfh*$^{-/-}$ and TRE2 *Cfh*$^{-/-}$ mouse strains were generated in-house. All mouse strains were either negative or backcrossed to become negative (*Thbs1*$^{-/-}$) for the *Pde6b*^{rd1}, *Gnat2*^{cpfl3}, and *Crb1*^{rd8} mutations that can lead to AMD-like features (Mattapallil et al., 2012). Mice were housed under specific pathogen-free condition, in a 12h/12h light/dark (100 lux) cycle with no additional cover in the cage, and with water and normal chow diet available *ad libitum*. All experimental protocols and procedures were approved by the local animal care ethics committee, "Comité d'éthique en expérimentation animale Charles Darwin" (N° Ce5/2010/011, Ce5/2010/044, Ce5/2011/033).

Choroidal and retinal flatmounts for mononuclear phagocyte and cone quantification

Eyes from male and female mice (as we never noticed a sex-dependent difference in subretinal MP accumulation in the past) (Combadiere et al., 2007; Hu et al., 2015; Levy et al., 2015a; Levy et al., 2015b; Sennlaub et al., 2013) were enucleated, fixed for 30 min in 4% PFA and sectioned at the limbus while the cornea and lens were discarded. The retinas were carefully peeled from the RPE/choroid/sclera. Retina and choroid were incubated with Peanut agglutinin Alexa 594 (Thermofisher; 1:50), anti-IBA-1 antibody (Wako chemicals; 1:400), , and anti-mouse cone-arrestin antibody (Millipore, #AB15282; 1:10 000) followed by secondary anti-rabbit antibody coupled to Alexa 488 and Alexa 647 (Thermo Fisher; 1:500) and nuclear staining using Hoechst. Choroids and retinas were flatmounted and viewed with a fluorescence microscope DM5500B (Leica). IBA-1^{+} cells were counted on whole RPE/choroidal flatmounts

and on the outer segment side of the retina. PA^{+}cone arrestin^{+} cells were counted on oriented retinal flatmounts in the central and peripheral retina.

Histology and Immunohistochemistry

Eyes were fixed in 0.5% glutaraldehyde, 4% PFA for 2h, dehydrated and mounted in Historesin (Leica). Oriented sections (5µm) crossing the inferior pole, optic nerve and superior pole were cut and stained with toluidin blue. Rows of nuclei in the outer nuclear layer (ONL) were counted at different distances from the optic nerve (Sennlaub et al., 2013). For immunohistochemistry, eyes from 4d light-challenged mice were fixed for 2h in 4% PFA, incubated in 30% sucrose overnight at 4°C, embedded in OCT and sectioned (10µm), and stained with anti-C3 antibody (clone 11H9 Hycult biotech; 1:50), anti-C3b/iC3b/C3c antibody (clone 3/26 Hycult biotech; 1:50), and anti-CFH antibody (ab8842 Abcam; 1:100) and appropriate secondary antibodies and Hoechst nuclear stain.

Light challenge model

Two- to three-months old male and female mice were adapted to darkness for 6 hours, pupils dilated daily and exposed to green LED light (starting at 2AM, 4500 Lux, JP Vezon Equipements) for 4 days and subsequently kept in cyclic 12h/12h normal facility conditions as previously described (Sennlaub et al., 2013). MP count was assessed at the end of light exposure (day 4) or 10 days later (day 14).

Hydrodynamic injection

Murine Complement Factor H was cloned into pLIVE vector (Mirus) using NheI and SacII restriction sites, so that, its expression was under the control of a mouse minimal albumin promoter. The construct was sequenced and the plasmid amplified with endotoxin-free Megaprep kits (Qiagen). Control groups were injected with the empty pLIVE plasmid and test groups with pLIVE expressing murine CFH. 100 µg of plasmid diluted in NaCl 0.9% were injected per mouse. The volume injected in the venous tail was 10% of the body weight (Rayes et al., 2010), which leads to robust transfection of the plasmid in the liver. Four days later, mice

were exposed to the light challenge model and 50µl of blood were taken (mandibular vein) at day 0, 4 and 14 to quantify plasma C3 concentration by ELISA (Innovative Research).

Monocyte and microglial cell preparations, analysis, and culture

Blood samples were collected for determination of plasma C3 (Innovative Research) and TSP-1 (Elabscience) levels by ELISA. Bone marrow monocytes, circulating monocytes , central nervous MC and retinal MC were purified. Mos were isolated by negative selection (EasySep Mouse Enrichment Kit, Stemcell Technologies). MCs were prepared from dissociated PBS-perfused brains or retinas (Neural Dissociation Kit, Miltenyi Biotec). After dissociation, 70µm filtered cell suspensions were washed and myelin was eliminated Percoll density gradient centrifugation. Then cells labeled with anti-CD11b microbeads (clone M1/70.15.11.5, Miltenyi Biotec) were purified by MS Columns (Miltenyi Biotec) and washed. No serum was used in any step of the purification to avoid cell contamination with serum derived CFH. The cells were used for adoptive transfer experiments, analyzed by RT-qPCR or cultured for 24h in serum free DMEM, in presence of recombinant human APOE3 (Interchim; 10µg/mL), and finally their supernatants were analyzed by cytokine multiplex array (MILLIPLEX MAP Mouse Cytokine/Chemokine Magnetic Bead Panel, Merck Millipore).

Subretinal adoptive mononuclear phagocyte transfer and clearance (Levy et al., 2015a)

Brain MCs, of the indicated male mouse strains were sorted as described above, labeled in 10µM CFSE (Thermo Fisher Scientific), washed and resuspended in PBS. They express the molecules of interest similarly to retinal MCs (Fig. S4, S6, and S7). 12000 cells (in 4µL) were injected in the subretinal space of anesthetized WT or *Cfh*$^{-/-}$ male mice (10-14 weeks old) using glass microcapillaries (Eppendorf) and a microinjector. A hole was pierced with the glass capillary prior to the injection in order to avoid intra-ocular pressure increase and to allow retinal detachment with 4µl of solution. The subretinal injection was verified by fundoscopy. In specific experiments, cells were co-injected with purified commercial human CFH

(500µg/ml; Tecomedical), purified native CFH_{Y402} and CFH_{402H} (500µg/ml, obtained from Claire Harris), recombinant CFH (500µg/ml, LFB Biotechnologies, Lille), recombinant human TSP-1 (10µg/ml, R&D Systems), anti-CD11b antibody (10µg/ml, clone 5C6 Abd Serotec), anti-C3b/iC3b/C3c antibody (10µg/ml, clone 3/26 Hycult biotech), isotype control rat IgG2 (10µg/ml, Invivogen), anti-TSP-1 antibody (10µg/ml, clone A4.1, Thermo Fisher), and isotype control mouse IgM (10µg/ml, Invivogen). Eyes were enucleated after 24 hours, fixed 30 minutes in PFA 4% and counterstained with Hoechst nuclear stain. Eyes with hemorrhages were discarded. $CFSE^+$ cells in the subretinal space were quantified on flatmounts on the RPE side of the retina and on the apical side of the RPE.

Thioglycollate induced peritonitis and flow cytometry

Intraperitoneal injections of 0.5 ml of 3% (wt/vol) thioglycollate (T 9032 Sigma Aldrich) broth were used to elicit peritonitis in male *Cfh*$^{-/-}$ mice and wildtype C57BL6/J controls. Where indicated, mice undergoing peritonitis were injected at day 1 with 100µl of PBS containing native or heat inactivated (1h at 96°C) purified commercial human CFH (500µg/ml; Tecomedical), recombinant human TSP-1 (50µg/ml, R&D Systems), the CD47-activating peptide PKHB1 (500µM) or the 4NGG control peptide (500µM), and exudate cells were analyzed at the indicated days.

At the indicated times, peritoneal lavage was performed after injecting 4 ml PBS containing 1% BSA and 0.5mM EDTA. Cells were labeled with antibodies directed against CD115 (clone AFS98), F4/80 (clone BM8), Gr-1 (anti-Ly6C and Ly-6G, clone RB6-8C5), ICAM-2 (clone 3C4), CD11b (M1/70) and MHC-II (clone M5/114.15.2). Antibodies were purchased from eBioscience. Cells suspensions were run on a BD Fortessa flow cytometer (BD biosciences) and analysis was performed using Flowjo software (TreeStar)

CFH binding assay by flow cytometry

Human CFH was conjugated to Cyanin 5.5 (Abcam conjugation kits). MCs from *Cx3cr1*$^{GFP/GFP}$ *Cfh*$^{-/-}$ were stained 30 minutes with Cy5.5-conjugated human CFH in PBS at indicated concentrations at 37°C and washed two times before acquisition on a BD Fortessa flow cytometer (BD biosciences). Analysis was performed using Flowjo software (TreeStar). Briefly, doublets were eliminated with FSC-H, FSC-W, SSC-H and SSC-W and microglial cells were identified as GFP^{high} cells. Bone marrow monocytes were blocked with anti CD16/CD32 antibodies (Seroblock, AbD Serotec) for 15 minutes, preincubated with control IgG or anti-CD11b antibody (clone 5C6, Abd Serotec) at 10µg/ml, and incubated with hCFH::Cy3 (with or without preincubation of IgG and anti CD11b 10µg/ml), were labeled with rat anti-CD115-PE (Abd Serotec), rat anti-Ly-6G AlexaFluor 700 (BD Biosciences) to be defined as GFP^{+}, CD115^{+}, Ly-6G^{-} cells. Note that the anti-CD11b clone M1/70.15.11.5 used for MC purification does not interfere with CFH binding as shown in Fig. 3A and the fact that recombinant CFH is capable to reverse the accelerated elimination of *Cx3cr1*$^{GFP/GFP}$ *Cfh*$^{-/-}$ MCs and *TRE2Cfh*$^{-/-}$ MCs sorted using clone M1/70 (Fig. 2). This difference is likely due to the fact clone M1/70 recognizes a distinct epitope of CD11b compared to the 5C6 clone (Rosen and Gordon, 1987).

Laser-injury model

Laser-coagulations were performed on male mice with an 532nm ophtalmological laser mounted on an operating microscope (Vitra Laser, 532nm, 450 mW, 50ms, and 250µm). Intravitreal injections of 2µl of PBS, recombinant human TSP-1 (10µg/ml), the 4NGG control peptide (200µM) and the PKHB1 CD47-activating peptide (200µM), anti-CD11b antibody (50µg/ml, clone 5C6 Abd Serotec), isotype control rat IgG2 (50µg/ml, Invivogen), were performed at day 4 and 7 using glass capillaries (Eppendorf) and a microinjector, and mice were sacrificed at day 10. RPE and retinal flatmounts were stained and quantified as previously described (Sennlaub et al., 2013) using polyclonal rabbit anti-IBA-1 (Wako) and rat anti-mouse

CD102 (clone 3C4, BD Biosciences) appropriate secondary antibodies and counterstained with Hoechst if indicated. Preparations were observed under a fluorescence microscope (DM5500, Leica) and IBA-1^{+} MPs on the RPE were counted in a diameter of 500µm around the CD102^{+} neovascularizations.

CD11b-CD47 proximity ligation assay

Mouse peritoneal exudate cells (PECs) were elicited by i.p. injection of 2 ml 3 % thioglycollate (T9032, Sigma) into 10 weeks old male C57BL/6J and *Cd47*$^{-/-}$ mice. After 1 day, PECs were isolated by flushing of the peritoneum with ice-cold PBS. Mφs were negatively selected by magnetic sorting following the protocol suggested by the manufacturer (EasySep Mouse Monocyte Enrichment Kit, Stemcell Technologies), then resuspended in X-VIVO 15 medium (Lonza) and plated in Lab-Tek® Chamber Slide™ (Nunc®). Brain *Cx3Cr1*$^{GFP/GFP}$ *Cfh*$^{-/-}$ MCs were prepared as described above, resuspended in X-VIVO 15 medium (Lonza) and plated in Lab-Tek® Chamber Slide™ similarly. After 2 h at 37 °C in a 5 % CO_2 atmosphere, cells were rinsed with PBS, fixed 10 minutes in 4% paraformaldehyde solution, rinsed and permeabilized by incubating cells 10 minutes in 0.1% Triton solution in PBS. Duolink® PLA assay was performed following the manufacturer's instructions (Sigma-Aldrich). In brief, rabbit anti-CD11b (ab75476, Abcam; 1:1000) and goat anti-CD47 (AF1866, R&D Systems; 1:1000) were incubated overnight at 4°C. Afterwards, anti-rabbit and anti-mouse oligonucleotides-labeled secondary antibodies (PLA probes) were incubated, followed by a ligase and polymerase reaction to amplify the signal. Images were taken on an Olympus FLUOVIEW FV1000 confocal laser-scanning microscope at imaging facility of the Institut de la Vision.

Statistical analysis

Sample sizes for our experiments were determined according to our previous studies(Combadiere et al., 2007; Hu et al., 2015; Levy et al., 2015a; Levy et al., 2015b; Sennlaub et al., 2013). Severe hemorrhage secondary to subretinal injection interferes with MP

clearance and was used as exclusion criteria. Graph Pad 6 (GraphPad Software) was used for data analysis and graphic representation. All values are reported as mean ± SEM. Statistical analysis and variance analysis was performed by one-way ANOVA followed by Bonferroni post-test (for multiple comparison) or Mann-Whitney U-test (2-group comparison) among means depending on the experimental design. The n and P-values are indicated in the figure legends.

References

Ambati, J., Atkinson, J.P., and Gelfand, B.D. (2013). Immunology of age-related macular degeneration. Nat Rev Immunol *13*, 438-451.

Anderson, D.H., Radeke, M.J., Gallo, N.B., Chapin, E.A., Johnson, P.T., Curletti, C.R., Hancox, L.S., Hu, J., Ebright, J.N., Malek, G.*, et al.* (2010). The pivotal role of the complement system in aging and age-related macular degeneration: hypothesis re-visited. Prog Retin Eye Res *29*, 95-112.

Appelboom, G., Piazza, M., Hwang, B.Y., Bruce, S., Smith, S., Bratt, A., Bagiella, E., Badjatia, N., Mayer, S., and Sander Connolly, E. (2011). Complement Factor H Y402H polymorphism is associated with an increased risk of mortality after intracerebral hemorrhage. J Clin Neurosci *18*, 1439-1443.

Chen, M., Copland, D.A., Zhao, J., Liu, J., Forrester, J.V., Dick, A.D., and Xu, H. (2012). Persistent inflammation subverts thrombospondin-1-induced regulation of retinal angiogenesis and is driven by CCR2 ligation. Am J Pathol *180*, 235-245.

Clark, S.J., Higman, V.A., Mulloy, B., Perkins, S.J., Lea, S.M., Sim, R.B., and Day, A.J. (2006). His-384 allotypic variant of factor H associated with age-related macular degeneration has different heparin binding properties from the non-disease-associated form. J Biol Chem *281*, 24713-24720.

Clark, S.J., Perveen, R., Hakobyan, S., Morgan, B.P., Sim, R.B., Bishop, P.N., and Day, A.J. (2010). Impaired binding of the age-related macular degeneration-associated complement factor H 402H allotype to Bruch's membrane in human retina. J Biol Chem *285*, 30192-30202.

Coffey, P.J., Gias, C., McDermott, C.J., Lundh, P., Pickering, M.C., Sethi, C., Bird, A., Fitzke, F.W., Maass, A., Chen, L.L.*, et al.* (2007). Complement factor H deficiency in aged mice causes retinal abnormalities and visual dysfunction. Proc Natl Acad Sci U S A *104*, 16651-16656.

Combadiere, C., Feumi, C., Raoul, W., Keller, N., Rodero, M., Pezard, A., Lavalette, S., Houssier, M., Jonet, L., Picard, E.*, et al.* (2007). CX3CR1-dependent subretinal microglia cell accumulation is associated with cardinal features of age-related macular degeneration. J Clin Invest *117*, 2920-2928.

Cruz-Guilloty, F., Saeed, A.M., Echegaray, J.J., Duffort, S., Ballmick, A., Tan, Y., Betancourt, M., Viteri, E., Ramkhellawan, G.C., Ewald, E.*, et al.* (2013). Infiltration of proinflammatory m1 macrophages into the outer retina precedes damage in a mouse model of age-related macular degeneration. Int J Inflam *2013*, 503725.

Dhillon, B., Wright, A.F., Tufail, A., Pappworth, I., Hayward, C., Moore, I., Strain, L., Kavanagh, D., Barlow, P.N., Herbert, A.P.*, et al.* (2010). Complement factor h autoantibodies and age-related macular degeneration. Invest Ophthalmol Vis Sci *51*, 5858-5863.

DiScipio, R.G., Daffern, P.J., Schraufstatter, I.U., and Sriramarao, P. (1998). Human polymorphonuclear leukocytes adhere to complement factor H through an interaction that involves alphaMbeta2 (CD11b/CD18). J Immunol *160*, 4057-4066.

Eandi, C.M., Charles Messance, H., Augustin, S., Dominguez, E., Lavalette, S., Forster, V., Hu, S.J., Siquieros, L., Craft, C.M., Sahel, J.A.*, et al.* (2016). Subretinal mononuclear phagocytes induce cone segment loss via IL-1beta. eLife *5*.

Fritsche, L.G., Chen, W., Schu, M., Yaspan, B.L., Yu, Y., Thorleifsson, G., Zack, D.J., Arakawa, S., Cipriani, V., Ripke, S.*, et al.* (2013). Seven new loci associated with age-related macular degeneration. Nat Genet *45*, 433-439, 439e431-432.

Fritsche, L.G., Fariss, R.N., Stambolian, D., Abecasis, G.R., Curcio, C.A., and Swaroop, A. (2014). Age-related macular degeneration: genetics and biology coming together. Annu Rev Genomics Hum Genet *15*, 151-171.
Fritsche, L.G., Igl, W., Bailey, J.N., Grassmann, F., Sengupta, S., Bragg-Gresham, J.L., Burdon, K.P., Hebbring, S.J., Wen, C., Gorski, M.*, et al.* (2016). A large genome-wide association study of age-related macular degeneration highlights contributions of rare and common variants. Nat Genet *48*, 134-143.
Gautier, E.L., Ivanov, S., Lesnik, P., and Randolph, G.J. (2013). Local apoptosis mediates clearance of macrophages from resolving inflammation in mice. Blood *122*, 2714-2722.
Gautier, E.L., Shay, T., Miller, J., Greter, M., Jakubzick, C., Ivanov, S., Helft, J., Chow, A., Elpek, K.G., Gordonov, S.*, et al.* (2012). Gene-expression profiles and transcriptional regulatory pathways that underlie the identity and diversity of mouse tissue macrophages. Nat Immunol *13*, 1118-1128.
Gilroy, D.W., Colville-Nash, P.R., Willis, D., Chivers, J., Paul-Clark, M.J., and Willoughby, D.A. (1999). Inducible cyclooxygenase may have anti-inflammatory properties. Nat Med *5*, 698-701.
Glass, C.K., Saijo, K., Winner, B., Marchetto, M.C., and Gage, F.H. (2010). Mechanisms underlying inflammation in neurodegeneration. Cell *140*, 918-934.
Griffith, T.S., Brunner, T., Fletcher, S.M., Green, D.R., and Ferguson, T.A. (1995). Fas ligand-induced apoptosis as a mechanism of immune privilege. Science *270*, 1189-1192.
Grivennikov, S.I., Greten, F.R., and Karin, M. (2010). Immunity, inflammation, and cancer. Cell *140*, 883-899.
Gupta, N., Brown, K.E., and Milam, A.H. (2003). Activated microglia in human retinitis pigmentosa, late-onset retinal degeneration, and age-related macular degeneration. Exp Eye Res *76*, 463-471.
Hageman, G.S., Anderson, D.H., Johnson, L.V., Hancox, L.S., Taiber, A.J., Hardisty, L.I., Hageman, J.L., Stockman, H.A., Borchardt, J.D., Gehrs, K.M.*, et al.* (2005). A common haplotype in the complement regulatory gene factor H (HF1/CFH) predisposes individuals to age-related macular degeneration. Proc Natl Acad Sci U S A *102*, 7227-7232.
Hotamisligil, G.S. (2010). Endoplasmic reticulum stress and the inflammatory basis of metabolic disease. Cell *140*, 900-917.
Hu, S.J., Calippe, B., Lavalette, S., Roubeix, C., Montassar, F., Housset, M., Levy, O., Delarasse, C., Paques, M., Sahel, J.A.*, et al.* (2015). Upregulation of P2RX7 in Cx3cr1-Deficient Mononuclear Phagocytes Leads to Increased Interleukin-1beta Secretion and Photoreceptor Neurodegeneration. J Neurosci *35*, 6987-6996.
Jimenez, B., Volpert, O.V., Crawford, S.E., Febbraio, M., Silverstein, R.L., and Bouck, N. (2000). Signals leading to apoptosis-dependent inhibition of neovascularization by thrombospondin-1. Nat Med *6*, 41-48.
Johnson, P.T., Betts, K.E., Radeke, M.J., Hageman, G.S., Anderson, D.H., and Johnson, L.V. (2006). Individuals homozygous for the age-related macular degeneration risk-conferring variant of complement factor H have elevated levels of CRP in the choroid. Proc Natl Acad Sci U S A *103*, 17456-17461.
Jones, L.L., and Tuszynski, M.H. (2002). Spinal cord injury elicits expression of keratan sulfate proteoglycans by macrophages, reactive microglia, and oligodendrocyte progenitors. J Neurosci *22*, 4611-4624.
Kang, Y.H., Urban, B.C., Sim, R.B., and Kishore, U. (2012). Human complement Factor H modulates C1q-mediated phagocytosis of apoptotic cells. Immunobiology *217*, 455-464.
Khandhadia, S., Hakobyan, S., Heng, L.Z., Gibson, J., Adams, D.H., Alexander, G.J., Gibson, J.M., Martin, K.R., Menon, G., Nash, K.*, et al.* (2013). Age-related Macular Degeneration and

Modification of Systemic Complement Factor H Production Through Liver Transplantation. Ophthalmology.
Kohno, H., Chen, Y., Kevany, B.M., Pearlman, E., Miyagi, M., Maeda, T., Palczewski, K., and Maeda, A. (2013). Photoreceptor Proteins Initiate Microglial Activation via Toll-like Receptor 4 in Retinal Degeneration Mediated by All-trans-retinal. J Biol Chem *288*, 15326-15341.
Kopp, A., Hebecker, M., Svobodova, E., and Jozsi, M. (2012). Factor h: a complement regulator in health and disease, and a mediator of cellular interactions. Biomolecules *2*, 46-75.
Lad, E.M., Cousins, S.W., Van Arnam, J.S., and Proia, A.D. (2015). Abundance of infiltrating CD163+ cells in the retina of postmortem eyes with dry and neovascular age-related macular degeneration. Graefes Arch Clin Exp Ophthalmol.
Levy, O., Calippe, B., Lavalette, S., Hu, S.J., Raoul, W., Dominguez, E., Housset, M., Paques, M., Sahel, J.A., Bemelmans, A.P.*, et al.* (2015a). Apolipoprotein E promotes subretinal mononuclear phagocyte survival and chronic inflammation in age-related macular degeneration. EMBO Mol Med *7*, 211-226.
Levy, O., Lavalette, S., Hu, S.J., Housset, M., Raoul, W., Eandi, C., Sahel, J.A., Sullivan, P.M., Guillonneau, X., and Sennlaub, F. (2015b). APOE-isoforms control pathogenic subretinal inflammation in age related macular degeneration. J Neurosci *35*, 13568 –13576.
Lim, H.Y., Muller, N., Herold, M.J., van den Brandt, J., and Reichardt, H.M. (2007). Glucocorticoids exert opposing effects on macrophage function dependent on their concentration. Immunology *122*, 47-53.
Losse, J., Zipfel, P.F., and Jozsi, M. (2010). Factor H and factor H-related protein 1 bind to human neutrophils via complement receptor 3, mediate attachment to Candida albicans, and enhance neutrophil antimicrobial activity. J Immunol *184*, 912-921.
Luo, C., Chen, M., and Xu, H. (2011). Complement gene expression and regulation in mouse retina and retinal pigment epithelium/choroid. Mol Vis *17*, 1588-1597.
Magnusson, K.P., Duan, S., Sigurdsson, H., Petursson, H., Yang, Z., Zhao, Y., Bernstein, P.S., Ge, J., Jonasson, F., Stefansson, E.*, et al.* (2006). CFH Y402H confers similar risk of soft drusen and both forms of advanced AMD. PLoS Med *3*, e5.
Manna, P.P., Dimitry, J., Oldenborg, P.A., and Frazier, W.A. (2005). CD47 augments Fas/CD95-mediated apoptosis. J Biol Chem *280*, 29637-29644.
Martin, M., and Blom, A.M. (2016). Complement in removal of the dead - balancing inflammation. Immunological reviews *274*, 218-232.
Martinez-Torres, A.C., Quiney, C., Attout, T., Boullet, H., Herbi, L., Vela, L., Barbier, S., Chateau, D., Chapiro, E., Nguyen-Khac, F.*, et al.* (2015). CD47 agonist peptides induce programmed cell death in refractory chronic lymphocytic leukemia B cells via PLCgamma1 activation: evidence from mice and humans. PLoS Med *12*, e1001796.
Mastellos, D., Prechl, J., Laszlo, G., Papp, K., Olah, E., Argyropoulos, E., Franchini, S., Tudoran, R., Markiewski, M., Lambris, J.D., and Erdei, A. (2004). Novel monoclonal antibodies against mouse C3 interfering with complement activation: description of fine specificity and applications to various immunoassays. Molecular immunology *40*, 1213-1221.
Mathis, T., Housset, M., Eandi, C., Beguier, F., Touhami, S., Reichman, S., Augustin, S., Gondouin, P., Sahel, J.A., Kodjikian, L.*, et al.* (2016). Activated monocytes resist elimination by retinal pigment epithelium and downregulate their OTX2 expression via TNF-alpha. Aging Cell.
Matsui, H., Ohgomori, T., Natori, T., Miyamoto, K., Kusunoki, S., Sakamoto, K., Ishiguro, N., Imagama, S., and Kadomatsu, K. (2013). Keratan sulfate expression in microglia is

diminished in the spinal cord in experimental autoimmune neuritis. Cell Death Dis *4*, e946.
Mattapallil, M.J., Wawrousek, E.F., Chan, C.C., Zhao, H., Roychoudhury, J., Ferguson, T.A., and Caspi, R.R. (2012). The rd8 mutation of the Crb1 gene is present in vendor lines of C57BL/6N mice and embryonic stem cells, and confounds ocular induced mutant phenotypes. Invest Ophthalmol Vis Sci *53*, 2921-2927.
Mihlan, M., Stippa, S., Jozsi, M., and Zipfel, P.F. (2009). Monomeric CRP contributes to complement control in fluid phase and on cellular surfaces and increases phagocytosis by recruiting factor H. Cell Death Differ *16*, 1630-1640.
Nathan, C., and Ding, A. (2010). Nonresolving inflammation. Cell *140*, 871-882.
Ng, T.F., and Streilein, J.W. (2001). Light-induced migration of retinal microglia into the subretinal space. Invest Ophthalmol Vis Sci *42*, 3301-3310.
Ng, T.F., Turpie, B., and Masli, S. (2009). Thrombospondin-1-mediated regulation of microglia activation after retinal injury. Invest Ophthalmol Vis Sci *50*, 5472-5478.
Penfold, P.L., Madigan, M.C., Gillies, M.C., and Provis, J.M. (2001). Immunological and aetiological aspects of macular degeneration. Prog Retin Eye Res *20*, 385-414.
Pfeiffer, A., Bottcher, A., Orso, E., Kapinsky, M., Nagy, P., Bodnar, A., Spreitzer, I., Liebisch, G., Drobnik, W., Gempel, K.*, et al.* (2001). Lipopolysaccharide and ceramide docking to CD14 provokes ligand-specific receptor clustering in rafts. Eur J Immunol *31*, 3153-3164.
Pickering, M.C., Cook, H.T., Warren, J., Bygrave, A.E., Moss, J., Walport, M.J., and Botto, M. (2002). Uncontrolled C3 activation causes membranoproliferative glomerulonephritis in mice deficient in complement factor H. Nat Genet *31*, 424-428.
Quesada, A.J., Nelius, T., Yap, R., Zaichuk, T.A., Alfranca, A., Filleur, S., Volpert, O.V., and Redondo, J.M. (2005). In vivo upregulation of CD95 and CD95L causes synergistic inhibition of angiogenesis by TSP1 peptide and metronomic doxorubicin treatment. Cell Death Differ *12*, 649-658.
Rayes, J., Hollestelle, M.J., Legendre, P., Marx, I., de Groot, P.G., Christophe, O.D., Lenting, P.J., and Denis, C.V. (2010). Mutation and ADAMTS13-dependent modulation of disease severity in a mouse model for von Willebrand disease type 2B. Blood *115*, 4870-4877.
Rayes, J., Roumenina, L.T., Dimitrov, J.D., Repesse, Y., Ing, M., Christophe, O., Jokiranta, T.S., Halbwachs-Mecarelli, L., Borel-Derlon, A., Kaveri, S.V.*, et al.* (2014). The interaction between factor H and VWF increases factor H cofactor activity and regulates VWF prothrombotic status. Blood *123*, 121-125.
Rosen, H., and Gordon, S. (1987). Monoclonal antibody to the murine type 3 complement receptor inhibits adhesion of myelomonocytic cells in vitro and inflammatory cell recruitment in vivo. J Exp Med *166*, 1685-1701.
Rutar, M., Natoli, R., and Provis, J.M. (2012). Small interfering RNA-mediated suppression of Ccl2 in Muller cells attenuates microglial recruitment and photoreceptor death following retinal degeneration. J Neuroinflammation *9*, 221.
Sakurai, E., Anand, A., Ambati, B.K., van Rooijen, N., and Ambati, J. (2003). Macrophage depletion inhibits experimental choroidal neovascularization. Invest Ophthalmol Vis Sci *44*, 3578-3585.
Sarks, S.H. (1976). Ageing and degeneration in the macular region: a clinico-pathological study. Br J Ophthalmol *60*, 324-341.
Schlaf, G., Demberg, T., Beisel, N., Schieferdecker, H.L., and Gotze, O. (2001). Expression and regulation of complement factors H and I in rat and human cells: some critical notes. Molecular immunology *38*, 231-239.
Sennlaub, F., Auvynet, C., Calippe, B., Lavalette, S., Poupel, L., Hu, S.J., Dominguez, E., Camelo, S., Levy, O., Guyon, E.*, et al.* (2013). CCR2(+) monocytes infiltrate atrophic lesions

in age-related macular disease and mediate photoreceptor degeneration in experimental subretinal inflammation in Cx3cr1 deficient mice. EMBO Mol Med *5*, 1775-1793.
Shaw, P.X., Zhang, L., Zhang, M., Du, H., Zhao, L., Lee, C., Grob, S., Lim, S.L., Hughes, G., Lee, J.*, et al.* (2012). Complement factor H genotypes impact risk of age-related macular degeneration by interaction with oxidized phospholipids. Proc Natl Acad Sci U S A *109*, 13757-13762.
Suzuki, M., Tsujikawa, M., Itabe, H., Du, Z.J., Xie, P., Matsumura, N., Fu, X., Zhang, R., Sonoda, K.H., Egashira, K.*, et al.* (2012). Chronic photo-oxidative stress and subsequent MCP-1 activation as causative factors for age-related macular degeneration. J Cell Sci *125*, 2407-2415.
Tedesco, D., and Haragsim, L. (2012). Cyclosporine: a review. J Transplant *2012*, 230386.
Thompson, C.L., Klein, B.E., Klein, R., Xu, Z., Capriotti, J., Joshi, T., Leontiev, D., Lee, K.E., Elston, R.C., and Iyengar, S.K. (2007). Complement factor H and hemicentin-1 in age-related macular degeneration and renal phenotypes. Hum Mol Genet *16*, 2135-2148.
Toomey, C.B., Kelly, U., Saban, D.R., and Bowes Rickman, C. (2015). Regulation of age-related macular degeneration-like pathology by complement factor H. Proc Natl Acad Sci U S A *112*, E3040-3049.
Tsutsumi, C., Sonoda, K.H., Egashira, K., Qiao, H., Hisatomi, T., Nakao, S., Ishibashi, M., Charo, I.F., Sakamoto, T., Murata, T., and Ishibashi, T. (2003). The critical role of ocular-infiltrating macrophages in the development of choroidal neovascularization. J Leukoc Biol *74*, 25-32.
Vaziri-Sani, F., Hellwage, J., Zipfel, P.F., Sjoholm, A.G., Iancu, R., and Karpman, D. (2005). Factor H binds to washed human platelets. J Thromb Haemost *3*, 154-162.
Wang, S., Sorenson, C.M., and Sheibani, N. (2012). Lack of thrombospondin 1 and exacerbation of choroidal neovascularization. Arch Ophthalmol *130*, 615-620.
Weismann, D., Hartvigsen, K., Lauer, N., Bennett, K.L., Scholl, H.P., Charbel Issa, P., Cano, M., Brandstatter, H., Tsimikas, S., Skerka, C.*, et al.* (2011). Complement factor H binds malondialdehyde epitopes and protects from oxidative stress. Nature *478*, 76-81.
Wilms, H., Wollmer, M.A., and Sievers, J. (1999). In vitro-staining specificity of the antibody 5-D-4 for microglia but not for monocytes and macrophages indicates that microglia are a unique subgroup of the myelomonocytic lineage. J Neuroimmunol *98*, 89-95.
Wong, W.L., Su, X., Li, X., Cheung, C.M., Klein, R., Cheng, C.Y., and Wong, T.Y. (2014). Global prevalence of age-related macular degeneration and disease burden projection for 2020 and 2040: a systematic review and meta-analysis. Lancet Glob Health *2*, e106-116.
Yehualaeshet, T., O'Connor, R., Green-Johnson, J., Mai, S., Silverstein, R., Murphy-Ullrich, J.E., and Khalil, N. (1999). Activation of rat alveolar macrophage-derived latent transforming growth factor beta-1 by plasmin requires interaction with thrombospondin-1 and its cell surface receptor, CD36. Am J Pathol *155*, 841-851.
Zhang, Z., Yu, D., Yuan, J., Guo, Y., Wang, H., and Zhang, X. (2012). Cigarette smoking strongly modifies the association of complement factor H variant and the risk of lung cancer. Cancer Epidemiol *36*, e111-115.

Figure Legends

Figure 1: CFH deficiency prevents chronic pathogenic subretinal inflammation

A and B: (A) Representative images of 12 month-old IBA-1 (green) stained RPE flatmounts of *Cx3cr1*$^{GFP/GFP}$ and *Cx3cr1*$^{GFP/GFP}$ *Cfh*$^{-/-}$ mice and (A and B) quantification of subretinal IBA-1^{+} MPs in 2-3 months and 12 months old mice of the indicated strains (A: one-way Anova/Bonferroni test *p<0,0001 versus all other groups, Mann Whitney $^{\$}$p<0.0001 versus *Cx3cr1*$^{GFP/GFP}$ at 12 months of age; B: one-way Anova/Bonferroni test *p<0,0001 versus all other groups, Mann Whitney $^{\$}$p=0.0003 versus *TRE2* at 12 months of age).

C-F: (C) Micrographs, taken 1000 µm from the optic nerve, of 12 month-old *Cx3cr1*$^{GFP/GFP}$ and *Cx3cr1*$^{GFP/GFP}$ *Cfh*$^{-/-}$ mice. (D) Photoreceptor nuclei rows at increasing distances (-3000µm: inferior pole, +3000µm: superior pole) from the optic nerve (0µm) in 12 month-old mice. (E and F) Quantification of the area under the curve of photoreceptor nuclei row counts of 12 month-old mice of the indicated transgenic mouse strains (E: one-way Anova/Bonferroni test: *p<0,0001 versus all other groups; Mann Whitney $^{\$}$p=0,0024 versus *Cx3cr1*$^{GFP/GFP}$ mice; F: one-way Anova/Bonferroni test: *p<0,001 versus all other groups; Mann Whitney $^{\$}$p=0,0158 versus *TRE2* mice).

G-J: (G) Micrographs, taken in the superior periphery of peanut agglutinin (staining cone segments, red), cone arrestin (white), IBA-1 (green) triple stained 12 month-old *Cx3cr1*$^{GFP/GFP}$ and *Cx3cr1*$^{GFP/GFP}$ *Cfh*$^{-/-}$ mice. (H) Cone density quantifications on retinal flatmounts in peripheral and central, inferior and superior retina (-3000µm: inferior pole, +3000µm: superior pole, optic nerve: 0µm) and their average (I and J) in 12 month-old mice of the indicated transgenic mouse strains (I: one-way Anova/Bonferroni test: *p<0,0001 versus all other groups; Mann Whitney $^{\$}$p=0,0024 versus *Cx3cr1*$^{GFP/GFP}$ mice; J: one-way Anova/Bonferroni test: *p<0,0001 versus all other groups; Mann Whitney $^{\$}$p=0,0158 versus *TRE2* mice).

TRE2 and *TRE3*: Targeted replacement mice expressing human APOE 2 and 3 isoforms
ONL: outer nuclear layer; Scale bar A and C = 50µm.

n= number of replicates indicated in the graphs; replicates represent quantifications of eyes from different mice of at least three different cages.

Figure 2: CFH inhibits the resolution of acute subretinal inflammation

A and B: (A) Representative images of IBA-1 (green) stained RPE flatmounts of light-challenged *TRE2* and *TRE2 Cfh*$^{-/-}$ mice and (A and B) quantification of subretinal IBA-1^{+} MPs in non-illuminated (NI), 4 days-light challenged (d4), and 4 days-light challenged followed by 10 days of recovery (d4+10) of 2-3 months old mice of the indicated strains. (A: one way Anova/Bonferroni test *p<0,0001 versus the NI groups and *TRE3* mice at d4, $^{\$}$p<0.0001 versus *TRE2* d4+10; MannWhitney $^{\$}$p=0,0004 versus *TRE2* at d4+10; B: one way Anova/Bonferroni test *p<0,0001 versus the NI groups and C57BL6/J mice at d4, $^{\$}$p<0.0001 versus *Cx3cr1*$^{GFP/GFP}$ at d4+10; MannWhitney $^{\$}$p=0,0002 versus *Cx3cr1*$^{GFP/GFP}$ at d4+10).

C: Quantification by ELISA of circulating plasma C3 in control animals and after hypervolemic liver transfection with a control plasmid (ctl Pl) or a plasmid encoding murine CFH (mCFH) in 2-3 months old *Cx3cr1*$^{GFP/GFP}$ and *Cx3cr1*$^{GFP/GFP}$ *Cfh*$^{-/-}$ mice. Measurements were performed before (d0), at the end (d4) and ten days after (d14) the light-challenge. (one way Anova/Bonferroni test at d0 *p=0,0003, d4 *p=0,0018, d4+10 *p=0,0009 compared to control plasmid injected mice at each time point).

D: Quantification of subretinal IBA-1^{+} MPs/mm^{2} in light-challenge model at day 14 in 2-3 month-old *Cx3cr1*$^{GFP/GFP}$ and *Cx3cr1*$^{GFP/GFP}$ *Cfh*$^{-/-}$ mice after hypervolemic liver transfection of the empty plasmid or the plasmid encoding murine CFH. (Mann Whitney = 0,1).

E: Quantitative RT-PCR of *Cfh* mRNA normalized to *Rps26* mRNA expression in retina, choroid/RPE, circulating monocytes (cMo), bone marrow monocytes (BM-Mo), retinal microglia (MC Retina) and brain microglia from the indicated strains (n=replicates from individual mice except for retinal MCs which represent 3 preparations from 5 pooled mice each).

F: Representative micrograph of CFSE^{+} MCs on RPE flatmounts of the indicated strains 24h after subretinal adoptive transfer to *Cfh*$^{-/-}$ mice. Quantification of CFSE^{+} MCs of the indicated strains 24h after adoptive transfer to WT C57BL6/J or *Cfh*$^{-/-}$ mice, with or without purified human CFH (one way Anova/Bonferroni test *p<0,001 versus C57BL6/J CFSE^{+} MCs in C57BL6/J recipients, $^{\$}$p=0,0043 versus *Cx3cr1*$^{GFP/GFP}$ CFSE^{+} MCs in C57BL6/J recipients, †p=0,0139 versus *Cx3cr1*$^{GFP/GFP}$ *Cfh*$^{-/-}$ CFSE^{+} MCs in C57BL6/J recipients; there were no significant differences between groups injected in WT C57BL6/J or *Cfh*$^{-/-}$ recipients for each cell genotype).

G: Quantification of subretinal CFSE^{+} MCs of the indicated strains 24h after adoptive transfer to C57BL6/J WT mice, with or without purified human CFH (one way Anova/Bonferroni test *p=0,0009 versus C57BL6/J CFSE^{+} MCs, $^{\$}$p=0,0012 versus *TRE2* CFSE^{+} MCs, †p=0,0085 versus *TRE2 Cfh*$^{-/-}$ CFSE^{+} MCs).

n=number of replicates presented in the graphs; for A, B and D n=replicates represent quantifications of eyes from different mice of at least three different cages; for F and G n=replicates from individual mice from three experiments with three different cell preparations. *TRE2* and *TRE3*: Targeted replacement mice expressing human APOE 2 and 3 isoforms; post-transf.: post-transfection; light-chall: light-challenge; ctlPL: control plasmid; mCFH: murine CFH plasmid; Scale bar A and F = 50µm.

Figure 3: CFH binding to CD11b/CD18 inhibits TSP-1/CD47 mediated MP elimination

A and B: Representative cytometry plots of (A) sorted brain *Cx3cr1*$^{GFP/GFP}$ *Cfh*$^{-/-}$ Microglial Cells (gated on GFP^{high}) incubated with increasing dose of hCFH::Cy5.5 (15,625µ/ml to 500µg/ml), and (B) sorted *Cx3cr1*$^{GFP/GFP}$ *Cfh*$^{-/-}$ bone marrow monocytes pre-incubated with an isotype IgG or anti-CD11b IgG (5C6 clone) before hCFH::Cy3 or PBS incubation. Bone marrow monocytes were gated as GFP^{+} CD115^{+} Ly-6G^{-} cells (the experiments were repeated three times with similar results).

C: Representative micrograph of subretinal *Cx3cr1*$^{GFP/GFP}$ *Cfh*$^{-/-}$ CFSE^{+} MCs on RPE flatmounts 24h after subretinal adoptive transfer injection together with CFH and control IgG or anti-CD11b IgG (clone 5C6) and *Cx3cr1*$^{GFP/GFP}$ CFSE^{+} MCs with control IgG, anti-CD11b IgG (clone 5C6) or anti-C3b/iC3b/C3c IgG (clone 3/26) to WT C57BL6/J mice and quantification of the indicated groups (Anova/Bonferroni test †p=0.0034 versus *Cx3cr1*$^{GFP/GFP}$ *Cfh*$^{-/-}$ CFSE^{+} MCs without CFH, ‡ p=0,0036 versus *Cx3cr1*$^{GFP/GFP}$ *Cfh*$^{-/-}$ + CFH + cIgG, Mann Whitney *p=0,0083 versus cIgG;).

D: Representative confocal micrographs of CD11b-CD47 complexes (red dots) detected by proximity ligation assay on freshly isolated brain *Cx3cr1*$^{GFP/GFP}$ *Cfh*$^{-/-}$ MCs counterstained with Hoechst nuclear stain (blue; negative control: omitting the primary antibodies; the experiment was repeated three times with similar results).

E: Quantification of subretinal CFSE^{+} MCs of the indicated strains 24h after adoptive transfer to WT C57BL6/J mice with and without recombinant TSP-1 (n=replicates from individual mice from experiments with three different cell preparations; one-way Anova/Bonferroni test ‡p=0,0359 versus C57BL6/J CFSE^{+} MCs without TSP-1; *p<0,0001 versus C57BL6/J CFSE^{+} MCs without TSP-1; $^{\$}$p<0.0001 versus *Tsp1*$^{-/-}$ CFSE^{+} MCs without TSP-1; †p=0,0002 versus C57BL6/J CFSE^{+} MCs without TSP-1).

F and G: Representative images of 12 month-old IBA-1 (green) stained RPE flatmounts of C57BL6/J and *Cd47*$^{-/-}$ mice and quantification of subretinal IBA-1^{+} MPs of WT C57BL6/J, *Thbds1*$^{-/-}$, *Cd47*$^{-/-}$ mice and *Cd36*$^{-/-}$ mice at (F) 2-3 months and 12 months and (G) after a 4 day-light challenge, followed by 10 days of recovery (n=replicates represent quantifications of eyes from different mice of at least three different experiments and cages; one-way Anova/Bonferroni test F: *p<0,0001 versus 2-3 months old *Thbds*1$^{-/-}$ mice and 12 months old C57BL6/J mice; †p <0,0001 versus 2-3 months old *Cd47*$^{-/-}$ mice and 12 months C57BL6/J mice; G: *p<0,0001 versus C57BL6/J; †p <0,0001 versus C57BL6/J).

H and I: Quantification of subretinal *Cx3cr1*$^{GFP/GFP}$ *Cfh*$^{-/-}$ CFSE^{+} MCs with (G) control IgM or anti-TSP-1 IgM (clone A4.1) 24h after adoptive transfer (Mann Whitney *p=0,0002 IgM versus anti-TSP-1) or (H) recombinant TSP-1 (rTSP1) and rTSP1 + purified CFH (one-way Anova/Bonferroni test $^{\$}$p=0,0024 versus *Cx3cr1*$^{GFP/GFP}$ *Cfh*$^{-/-}$ CFSE^{+} MCs without rTSP1; *p=0,0003 versus *Cx3cr1*$^{GFP/GFP}$ *Cfh*$^{-/-}$ CFSE^{+} MCs + rTSP).

J-L: (I) Representative micrographs of RPE flatmounts of CD102 (red) and IBA-1 (green) immunohistochemistry and quantification of subretinal IBA-1^{+} MPs on the RPE counted at a distance of 0-500µm from CD102^{+} CNV 10 days after the laser-injury in 2 month-old *Cx3cr1*$^{GFP/GFP}$ mice injected at day 4 and day 7 with (I) PBS or rTSP1, (J) control peptide 4NGG or CD47-activating peptide PKHB1, and (K) control IgG or anti-CD11b IgG (Mann Whitney I *p=0,0097; J *p<0,0001; K *p=0,0298)

Thbs: thrombospondin 1 gene; TSP-1: thrombospondin. n=number of replicates indicated in the graphs, for C, E, G and H n=replicates from individual mice from experiments with three different cell preparations, for F, I and J n=replicates represent quantifications of eyes from different mice of at least three different experiments and cages. Scale bar: C, F and I = 50µm; D left panels =20µm, right panel =10µm.

Figure 4: CFH inhibits the resolution of acute sterile peritonitis

A: Normalized signal intensity for Cfh mRNA levels extracted from Affymetrix transcription analysis of bone marrow monocytes (1), Ly-6C^{+} circulating blood monocytes (2), MHC-II^{-} and MHC-II^{+} monocyte-derived peritoneal macrophages at day 5 of thioglycollate-induced peritonitis in 3 months old WT C57BL6/J mice (3 and 4; one-way Anova/Bonferroni test †p=0,0036 versus blood monocytes; *p=0,0005 versus blood monocytes).

B: Representative cytometry plots of WT C57BL6/J (upper panels) or *Cfh*$^{-/-}$ mice (lower panels) three days after thioglycollate-induced peritonitis. CD115^{+} F4/80^{+} cells represents macrophages, with CD115^{+} F4/80^{+} ICAM-2^{lo} representing Mo-derived Mφ and CD115^{+} F4/80^{+} ICAM-2^{hi} representing resident macrophages.

C: Quantification of CD115^{+} F4/80^{+} ICAM-2^{lo} Mo-derived Mφ in exudates of WT C57BL6/J and *Cfh*$^{-/-}$ mice at indicated time points after thioglycollate-induced peritonitis (one-way Anova/Bonferroni test †p=0,012 versus d0 WT C57BL6/J; *p=0,005 versus d0 *Cfh*$^{-/-}$; p=0,9697 between d1 groups; $^{\$}$p<0,0001 versus d3 WT C57BL6/J).

D: Quantification of CD115^{+} F4/80^{+} ICAM-2^{lo} Mo-derived Mφ in exudates of *Cfh*$^{-/-}$ mice at day 2 (d2) after mice were injected with native (CFH) or heat-denatured (dCFH) purified CFH at day 1 (d1) (MannWhitney *p=0,0087 versus dCFH).

E: Representative confocal micrographs of CD11b-CD47 complexes (red dots) detected by proximity ligation assay on freshly harvested Mo-derived Mφ 1 day after thioglycollate injection in WT C57BL6/J and *Cd47*$^{-/-}$ mice. Hoechst was used for nuclear stain (blue; negative control: omitting the primary antibodies; the experiment was repeated three times with similar results).

F: Quantification of CD115^{+} F4/80^{+} ICAM-2^{lo} Mo-derived Mφ in exudates of WT C57BL6/J mice at day 2 after mice were injected with PBS or rTSP-1 (Mann Whitney $^{\$}$p=0,0048); or control peptide 4NGG or CD47-activating peptide PKHB1 (Mann Whitney $^{\$}$p=0,0087) at day 1.

Mφ: macrophage; Mo: monocyte; Thio: thioglycollate; MHC: major histocompatibility complex; dCFH: heat-denatured CFH; negCTL: negative control. n= number of replicates indicated in the graphs; replicates represent quantifications of exudate cells from different mice of three (C) or two (E and F) different peritonitis inductions. Scale bar: E=10µm.

Figure 5: The CFH_{402H} variant inhibits subretinal MC elimination more potently than the CFH_{Y402} form.

A: Quantification of subretinal *Cx3cr1*$^{GFP/GFP}$ *Cfh*$^{-/-}$ $CFSE^{+}$ monocytes on RPE and retinal flatmounts 24h after adoptive transfer to WT C57BL6/J mice with and without purified CFH_{Y402} or CFH_{402H} (Anova/Bonferroni test $^{*}p<0,0001$)

B: Quantification of subretinal *Cx3cr1*$^{GFP/GFP}$ *Cfh*$^{-/-}$ $CFSE^{+}$ microglial cells on RPE and retinal flatmounts 24h after adoptive transfer to WT C57BL6/J mice with and without purified CFH_{Y402} or CFH_{402H} (Anova/Bonferroni test $^{*}p=0,0025$ versus without CFH; $^{\dagger}p=0,0052$ versus CFH_{Y402}).

C: Quantification of subretinal *Cx3cr1*$^{GFP/GFP}$ *Cfh*$^{-/-}$ $CFSE^{+}$ microglial cells on RPE and retinal flatmounts 24h after adoptive transfer to WT C57BL6/J mice without or with recombinant TSP-1 (rTSP1), rTSP1 + recombinant CFH_{Y402} or rTSP1 + recombinant CFH_{402H} (Anova/Bonferroni test $^{\$}p=0,00236$ versus without TSP-1; $^{\dagger}p=0,0002$ versus with TSP-1;$^{\ddagger}p=0,0005$ versus with TSP-1 + CFH_{Y402}).

Mos: monocytes; MCs: microglial cells; rTSP1: recombinant TSP-1; n=number of replicates indicated in the graphs, replicates represent quantifications from individual mice from two (A) to three (B and C) experiments with three different cell preparations.

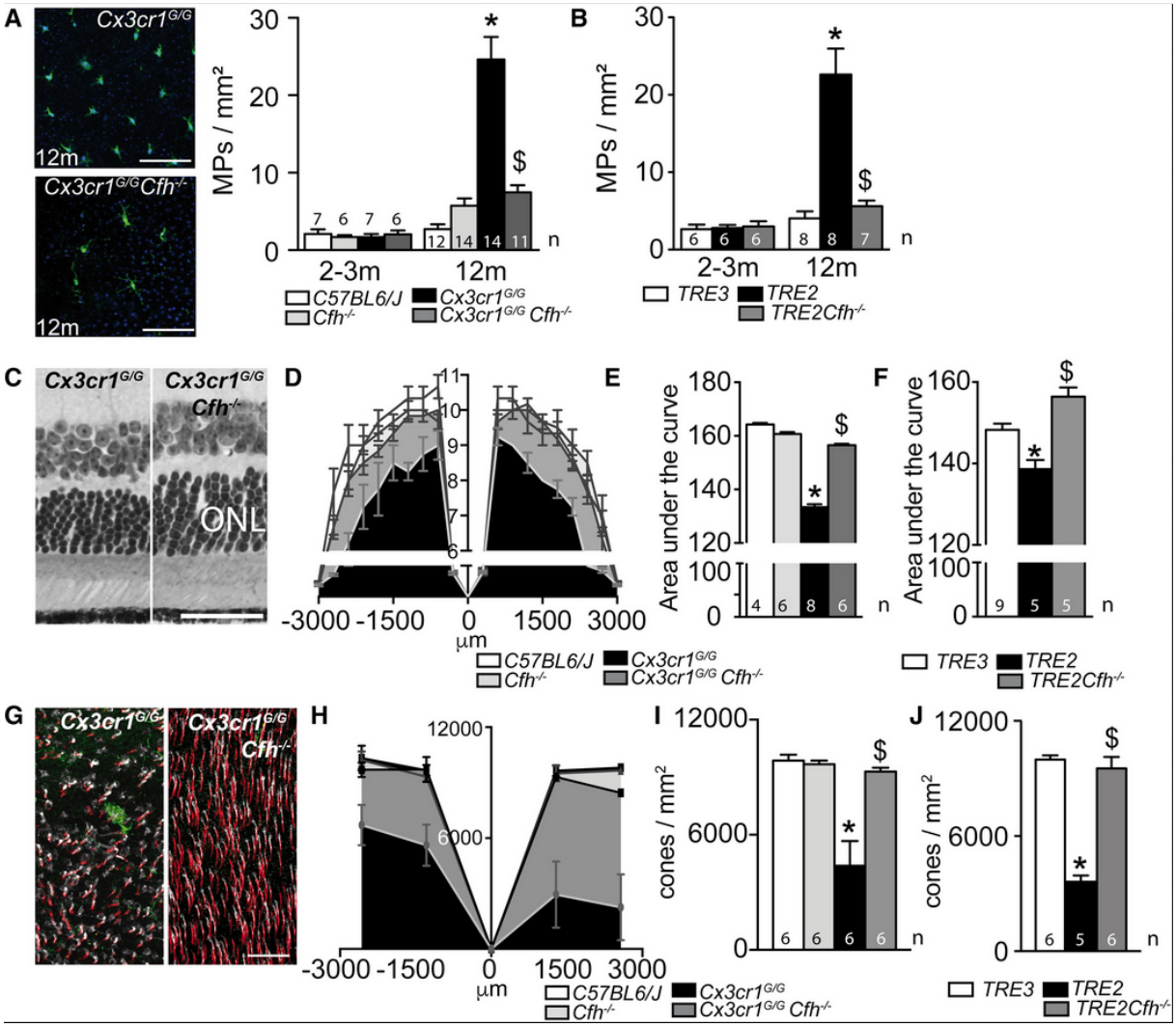
A
Cx3cr1G/G
12m
Cx3cr1G/G Cfh-/-
12m
MPs / mm²
30
20
10
0
*
$
7 6 7 6
12 14 14 11
n
2-3m
12m
C57BL6/J
Cfh-/-
Cx3cr1G/G
Cx3cr1G/G Cfh-/-
B
MPs / mm²
30
20
10
0
*
$
6 6 6
8 8 7
n
2-3m
12m
TRE3
TRE2
TRE2Cfh-/-
C
Cx3cr1G/G
Cx3cr1G/G Cfh-/-
ONL
D
11
10
9
8
7
6
-3000 -1500 0 1500 3000
µm
C57BL6/J
Cfh-/-
Cx3cr1G/G
Cx3cr1G/G Cfh-/-
E
Area under the curve
180
160
140
120
100
0
*
$
4 6 8 6
n
F
Area under the curve
160
140
120
100
0
*
$
9 5 5
n
TRE3
TRE2
TRE2Cfh-/-
G
Cx3cr1G/G
Cx3cr1G/G Cfh-/-
H
12000
6000
-3000 -1500 0 1500 3000
µm
C57BL6/J
Cfh-/-
Cx3cr1G/G
Cx3cr1G/G Cfh-/-
I
cones / mm²
12000
6000
0
*
$
6 6 6 6
n
J
cones / mm²
12000
6000
0
*
$
6 5 6
n
TRE3
TRE2
TRE2Cfh-/-

Figure 1

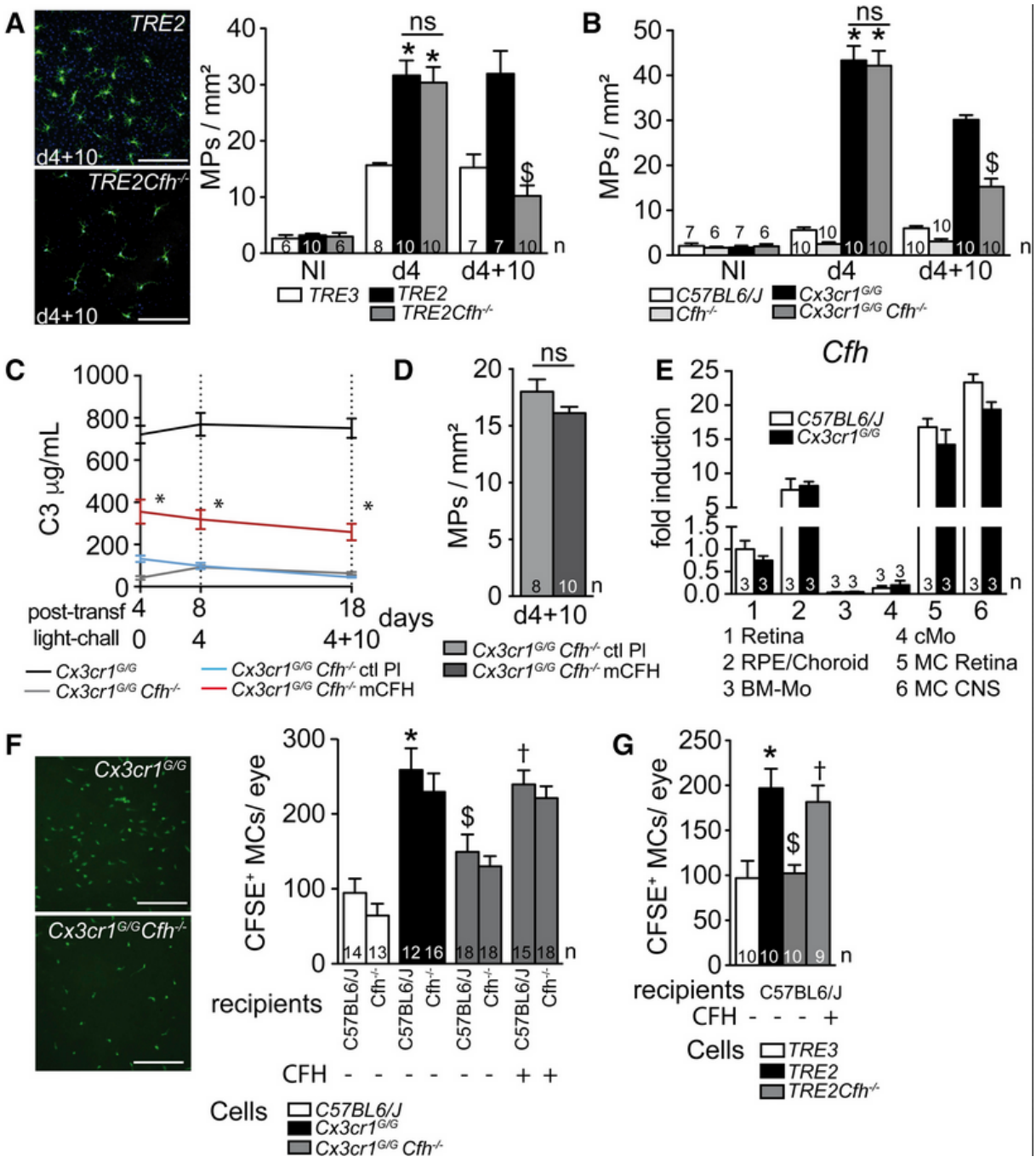
A
TRE2
d4+10
TRE2Cfh-/-
d4+10
MPs / mm²
ns
NI
d4
d4+10
n
TRE3
TRE2
TRE2Cfh-/-
B
MPs / mm²
ns
NI
d4
d4+10
n
C57BL6/J
Cfh-/-
Cx3cr1G/G
Cx3cr1G/G Cfh-/-
C
C3 µg/mL
post-transf
light-chall
days
Cx3cr1G/G
Cx3cr1G/G Cfh-/-
Cx3cr1G/G Cfh-/- ctl PI
Cx3cr1G/G Cfh-/- mCFH
D
MPs / mm²
ns
d4+10
n
Cx3cr1G/G Cfh-/- ctl PI
Cx3cr1G/G Cfh-/- mCFH
E
Cfh
fold induction
C57BL6/J
Cx3cr1G/G
n
1 Retina
2 RPE/Choroid
3 BM-Mo
4 cMo
5 MC Retina
6 MC CNS
F
Cx3cr1G/G
Cx3cr1G/GCfh-/-
CFSE+ MCs/ eye
recipients
C57BL6/J
Cfh-/-
CFH
Cells
C57BL6/J
Cx3cr1G/G
Cx3cr1G/G Cfh-/-
G
CFSE+ MCs/ eye
recipients
C57BL6/J
CFH
Cells
TRE3
TRE2
TRE2Cfh-/-

Figure 2

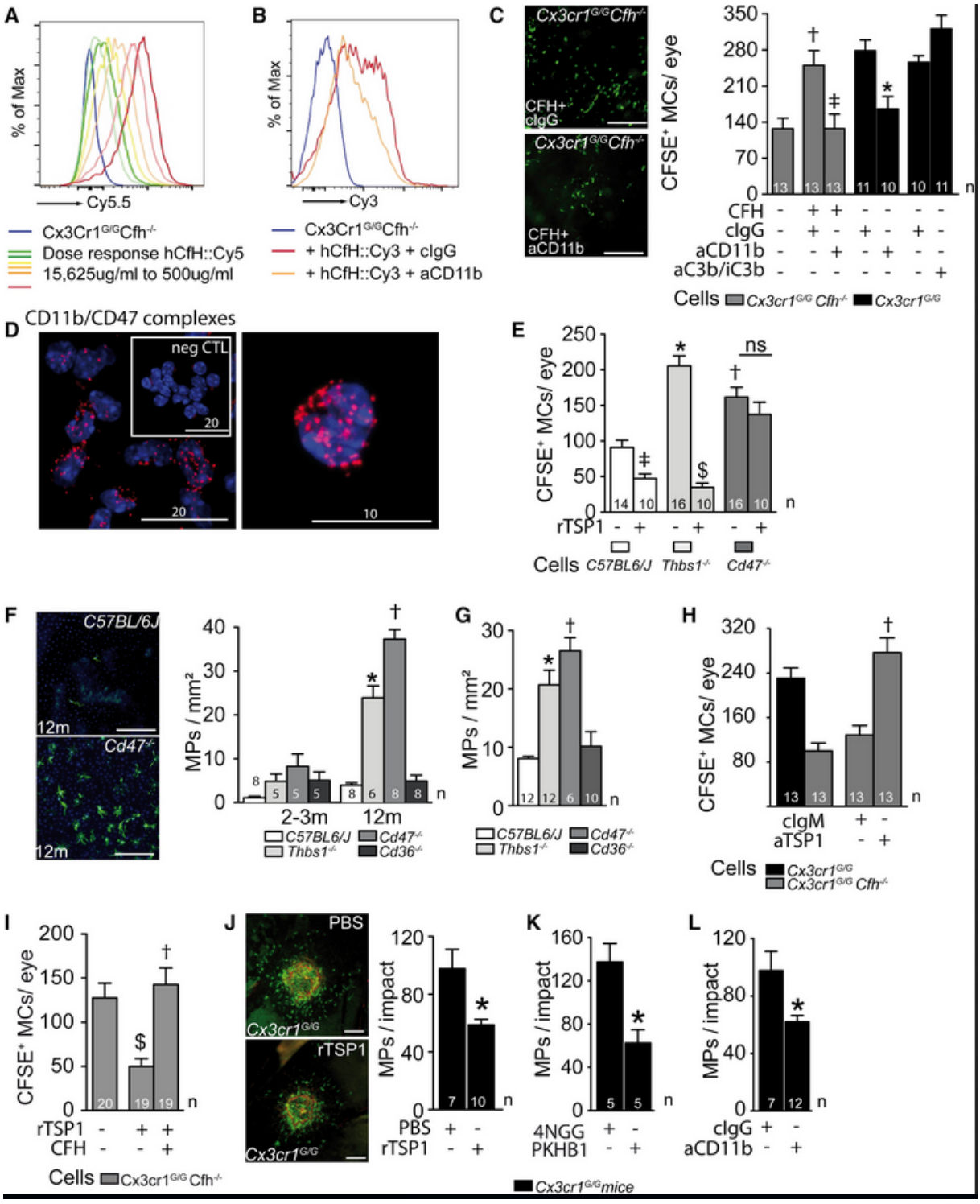
A
% of Max
Cy5.5
Cx3Cr1G/GCfh-/-
Dose response hCfH::Cy5
15,625ug/ml to 500ug/ml
B
% of Max
Cy3
Cx3Cr1G/GCfh-/-
+ hCfH::Cy3 + cIgG
+ hCfH::Cy3 + aCD11b
C
Cx3cr1G/GCfh-/-
CFH+ cIgG
Cx3cr1G/GCfh-/-
CFH+ aCD11b
CFSE+ MCs/ eye
CFH
cIgG
aCD11b
aC3b/iC3b
Cells Cx3cr1G/G Cfh-/- Cx3cr1G/G
D
CD11b/CD47 complexes
neg CTL
E
CFSE+ MCs/ eye
rTSP1
Cells C57BL6/J Thbs1-/- Cd47-/-
F
C57BL/6J
12m
Cd47-/-
12m
MPs / mm2
2-3m
12m
C57BL6/J
Cd47-/-
Thbs1-/-
Cd36-/-
G
MPs / mm2
C57BL6/J
Cd47-/-
Thbs1-/-
Cd36-/-
H
CFSE+ MCs/ eye
cIgM
aTSP1
Cells Cx3cr1G/G
Cx3cr1G/G Cfh-/-
I
CFSE+ MCs/ eye
rTSP1
CFH
Cells Cx3cr1G/G Cfh-/-
J
PBS
Cx3cr1G/G
rTSP1
Cx3cr1G/G
MPs / impact
PBS
rTSP1
K
MPs / impact
4NGG
PKHB1
L
MPs / impact
cIgG
aCD11b
Cx3cr1G/Gmice

Figure 3

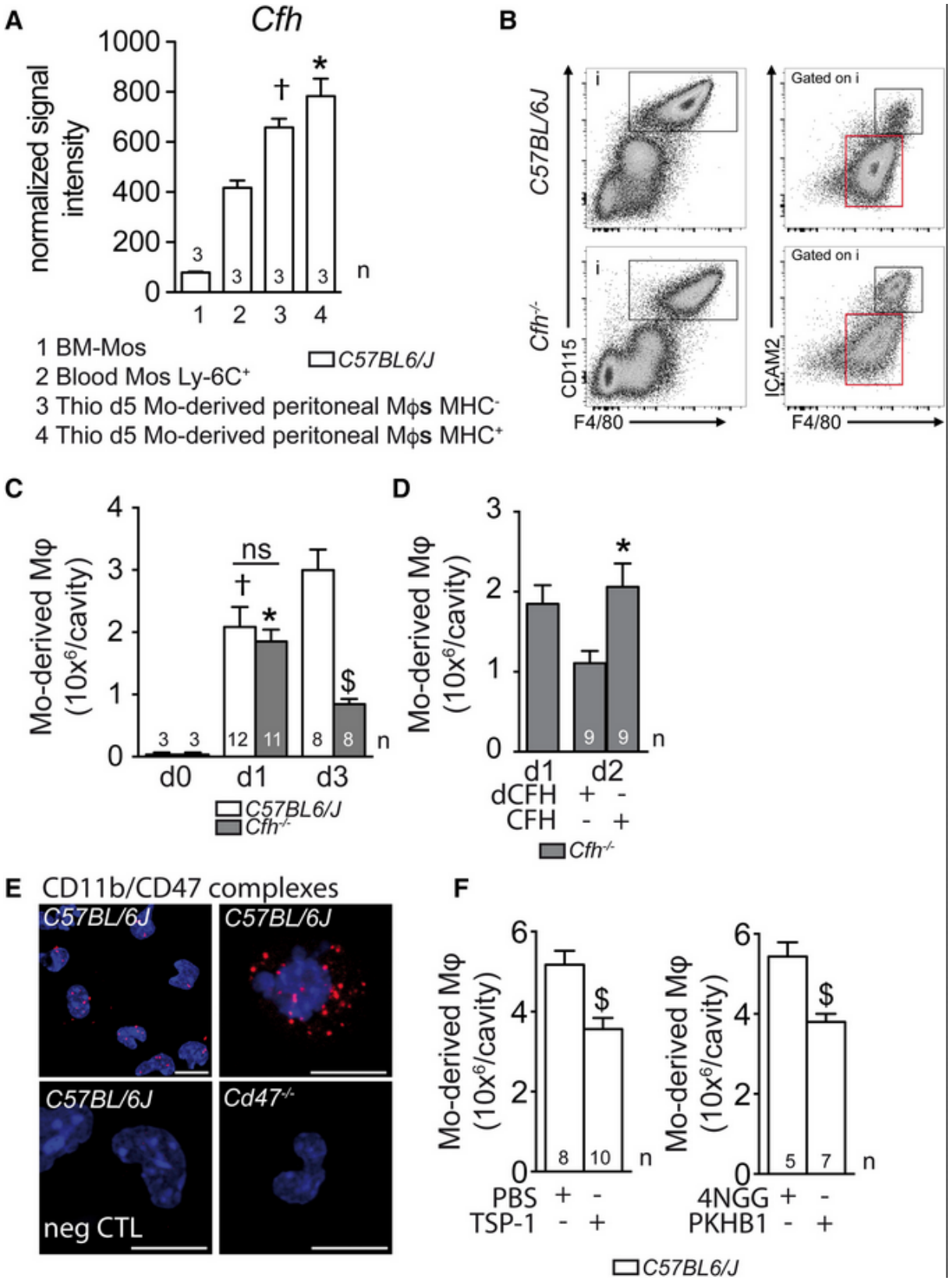
A
Cfh
normalized signal intensity
1000
800
600
400
200
0
3
3
3
3
n
1
2
3
4
*
†
1 BM-Mos
2 Blood Mos Ly-6C+
3 Thio d5 Mo-derived peritoneal Mϕs MHC-
4 Thio d5 Mo-derived peritoneal Mϕs MHC+
C57BL/6J
B
C57BL/6J
Cfh-/-
CD115
F4/80
i
Gated on i
ICAM2
C
Mo-derived Mφ (10x6/cavity)
ns
†
*
$
3
3
12
11
8
8
n
d0
d1
d3
C57BL/6J
Cfh-/-
D
Mo-derived Mφ (10x6/cavity)
*
9
9
n
d1
d2
dCFH + -
CFH - +
Cfh-/-
E
CD11b/CD47 complexes
C57BL/6J
C57BL/6J
C57BL/6J
neg CTL
Cd47-/-
F
Mo-derived Mφ (10x6/cavity)
$
8
10
n
PBS + -
TSP-1 - +
5
7
4NGG + -
PKHB1 - +
C57BL/6J

Figure 4

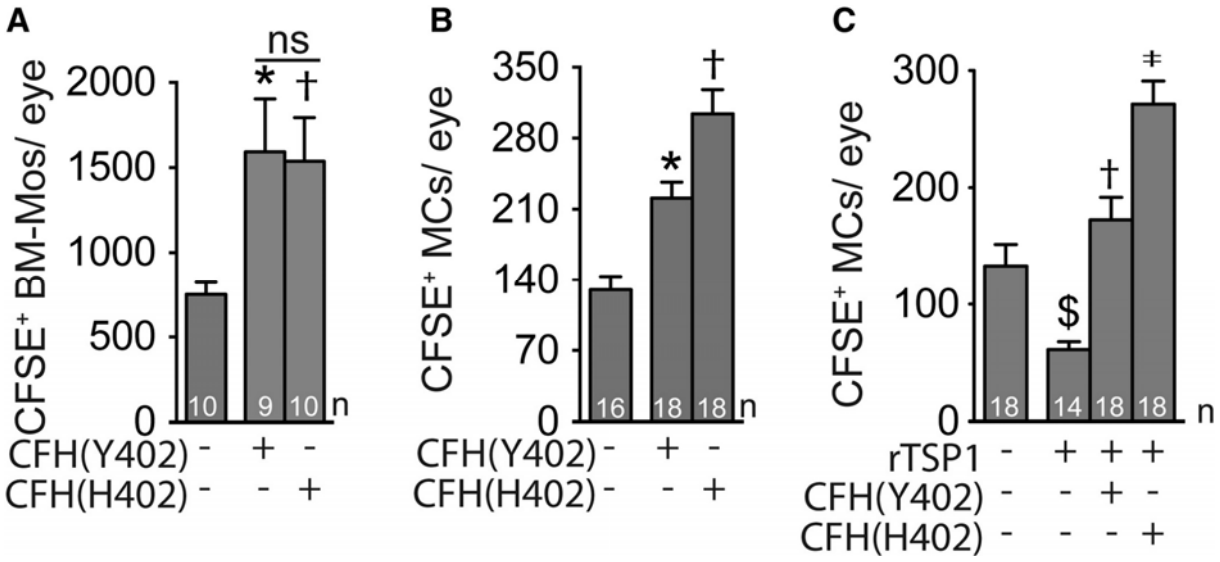
A
CFSE+ BM-Mos/ eye
2000
1500
1000
500
0
ns
*
†
10
9
10
n
CFH(Y402) - + -
CFH(H402) - - +
B
CFSE+ MCs/ eye
350
280
210
140
70
0
*
†
16
18
18
n
CFH(Y402) - + -
CFH(H402) - - +
C
CFSE+ MCs/ eye
300
200
100
0
$
†
‡
18
14
18
18
n
rTSP1 - + + +
CFH(Y402) - - + -
CFH(H402) - - - +

Figure 5

Figure S1: CFH-deficiency does not alter *in vitro* pathogenic cytokine secretion of microglial cells and monocytes.

We previously showed that MP derived IL-1β, IL-6, and TNFα induce photoreceptor degeneration and deregulate RPE-cell functions (Eandi et al., 2016; Hu et al., 2015; Levy et al., 2015a; Mathis et al., 2016). Cytokine multiplex analysis of supernatants from cultured primary bone marrow monocytes (BM-Mos, 100 000 cells/well) and brain microglial cells (MCs, 200 000 cells/well), incubated for 24 h in serum free DMEM medium or stimulated with APOE3 (5 µg/ml as previously described (Levy et al., 2015b)) of *Cx3cr1*$^{GFP/GFP}$ and *Cx3cr1*$^{GFP/GFP}$ *Cfh*$^{-/-}$ mice revealed no significant CFH-dependent differences in the secretion of these pathogenic cytokines in basal or stimulated conditions, suggesting that CFH did not significantly affect the secretion of these cytokines.

Figure S2: Plasma C3 concentrations and C3, and C3 fragment, and CFH immunohistochemistry in the transgenic mice.

A: Complement factor C3 (C3)-ELISA measurements of plasma C3 concentrations from the indicated mouse strains indicate that C3 plasma levels in *Cx3cr1*$^{GFP/GFP}$ mice do not differ from WT C57BL6/J mice and TRE2 mice from TRE3 mice and *Cfh*-deficiency induces low circulating levels of C3 in both strains, likely due to un-inhibited plasma complement activation and exhaustion (Pickering et al., 2002).

B-D: Immunohistochemistry (red) for C3 (B, clone 11H9 Hycult biotech), C3b/iC3b/C3c (C, clone 3/26 Hycult biotech), and CFH (A, ab8842 Abcam) in 4d light-challenged *Cx3cr1*$^{GFP/GFP}$ and *Cx3cr1*$^{GFP/GFP}$ *Cfh*$^{-/-}$ mice (GFP in green, nuclear stain in blue). (B) C3 was strongly detected in the choriocapillaries (arrow) of *Cx3cr1*$^{GFP/GFP}$mice, but not in and around subretinal MPs. In *Cx3cr1*$^{GFP/GFP}$ *Cfh*$^{-/-}$ mice that are characterized by low plasma C3 levels the signal in the choriocapillaries (adjacent to the RPE) was reduced. (C) Immunohistochemistry using the anti-mouse-C3b/iC3b/C3c antibody (clone 26/3 (Mastellos et al., 2004)) that specifically recognizes C3b and its fragments revealed a faint staining in the choriocapillaries (arrows), but no staining in the subretinal space of both mouse strains. (D) CFH was detected surrounding subretinal MPs (arrows), RPE and in the choriocapillaries (arrow head) in *Cx3cr1*$^{GFP/GFP}$, but not in *Cx3cr1*$^{GFP/GFP}$ *Cfh*$^{-/-}$ mice.

ONL: outer nuclear layer; RPE retinal pigment epithelium. negative control: omitting the primary antibodies revealed no staining (not shown); the experiment was repeated three times with similar results. Scale bar = 50µm.

Figure S3: *Cfh* induction in monocytes *in vitro* and monocyte elimination after subretinal adoptive transfer.

A: Quantitative RT-PCR of *Cfh* mRNA normalized with *Rps26* mRNA in WT C57BL6/J or *Cx3cr1*$^{GFP/GFP}$ monocytes cultivated for 18 h with or without photoreceptor outer segments to simulate the subretinal environment (POSs, one way Anova/Bonferroni test *p=0,0082 versus C57BL6/J Monocytes without POS, †p<0,0001 versus C57BL6/J Monocytes with and without POS). *Cfh* mRNA is robustly induced in BM-Mos from WT C57BL6/J-, and even more so from *Cx3cr1*$^{GFP/GFP}$-mice in contact with POS.

B: Representative micrograph of CFSE^{+} Monocytes on RPE flatmounts of the indicated strains 24h after subretinal adoptive transfer to *Cfh*$^{-/-}$ mice. Quantification of CFSE^{+} Mos of the indicated strains 24h after adoptive transfer to *Cfh*$^{-/-}$ mice (one way Anova/Bonferroni test *p<0,001 versus C57BL6/J CFSE^{+} Mos, $^{\$}$p=0,0043 versus *Cx3cr1*$^{GFP/GFP}$ CFSE^{+} Mos, †p=0,0178 versus *Cx3cr1*$^{GFP/GFP}$ *Cfh*$^{-/-}$ CFSE^{+} Mos).

POS: photoreceptor outer segments, Mos: monocytes; n=number of replicates indicated in the graphs, for A n=replicates represent different culture wells of the indicated conditions, the experiment was repeated twice with similar results; for B n=replicates from individual mice from two experiments with two different cell preparations. Scale bar B = 50µm.

Figure S4: Complement component expression in retina, liver, and MPs.

Quantitative RT-PCR of *Cfh* (A-C), *C3* (D-E), *Cfb* (G-I), and *Cfi* (J-K) mRNA, normalized with *Rps26* mRNA, in retina (1), retina without MCs (2, after sorting of MCs), liver (3), bone marrow monocytes (BM-Mo), retinal microglia (5, MC Retina) and brain microglia (6, CNS MC) from WT C57BL6/J mice (left column), and of BM-Mo, and MCs from retina and CNS of the indicated mouse strains (middle and right column). (A) MCs robustly expressed *Cfh* mRNA (~1/4 of liver expression level) significantly (~20-40 fold) more than BM-Mo (B and C). In contrast, *C3* mRNA was found in BM-Mos (B, ~1/60 of liver expression level), significantly (~50 fold) more than in MCs (E and F). Cfb mRNA transcription in MPs was detectable (~1/1000 of liver expression level, G) in all MPs with a relatively stronger expression in MCs (H and I). Interestingly, *Cfi* mRNA, robustly expressed in the liver (J), but was not detectable in MPs (K and L). Retinal and CNS MCs expressed the transcripts similarly and except for *Cfh* mRNA in $Cfh^{-/-}$ strains, we did not detect strain-dependent differences in the MPs.

BM-Mo: bone marrow monocytes; MC: microglial cell. CNS: central nervous system. A, D, G, and J n= replicates from individual mice; B, C, E, F, H, I, K, and L n= replicates from mRNA pooled from two individual mice.

Supplementary Figure 5: Cd11b, Cd18, *Cd47* and *Thbs1* transcription in MPs and TSP-1 plasma levels of the transgenic mice.

Quantitative RT-PCR of *Cd11b* (A-C), *Cd18* (D-E), *Cd47* (G-I), and *Thbs1* (J-L) mRNA, normalized with *Rps26* mRNA, in retina (1), retina without MCs (2, after sorting of MCs), liver (3), bone marrow monocytes (BM-Mo), retinal microglia (5, MC Retina) and brain microglia (6, CNS MC) from WT C57BL6/J mice (left column), and of BM-Mo, and MCs from retina and CNS of the indicated mouse strains (middle and right column). Both, *Cd11b* and *Cd18* mRNA were expressed specifically in MPs and not detected in mRNA from retina without the MC population (A and D). While *Cd11b* mRNA was more strongly expressed in MCs than in BM-Mo, no significant difference was detected in *Cd18* transcription (B, C, E, and F). (G-I): *Cd47* mRNA was expressed ubiquitously with a tendentiously higher expression in MCs compared to BM-Mos (C57BL6/J-, $Cx3cr1^{GFP/GFP}$, $Cx3cr1^{GFP/GFP}$ $Cfh^{-/-}$ mice). (J-L) *Thbs1* mRNA expression was more strongly expressed in MCs than in BM-Mo of C57BL6/J-, $Cx3cr1^{GFP/GFP}$, $Cx3cr1^{GFP/GFP}$ $Cfh^{-/-}$ mice, with differences less marked in TRE3- versus TRE2-mice. Retinal and CNS MCs expressed the transcripts similarly and we did not detect strain-dependent differences in the MPs.

(M and L) TSP-1 plasma concentrations of the indicated mouse strains measured by Elisa.

BM-Mo: bone marrow monocytes; MC: microglial cell. CNS: central nervous system. A, D, G, J, M, and N n= replicates from individual mice; B, C, E, F, H, I, K, and L n= replicates from mRNA pooled from two individual mice.